# Electrostatics of soft (bio)interfaces: Corrections of mean-field Poisson-Boltzmann theory for ion size, dielectric decrement and ion-ion correlations

Nicolas Lesniewska, Audrey Beaussart, Jérôme F.L. Duval

# Electrostatics of soft (bio)interfaces: corrections of mean-field Poisson-Boltzmann theory for ion size, dielectric decrement and ion-ion correlations.

Nicolas Lesniewska*, Audrey Beaussart, Jérôme F.L. Duval*

Université de Lorraine, CNRS, Laboratoire Interdisciplinaire des Environnements Continentaux (LIEC), UMR7360, Vandoeuvre-lès-Nancy F-54500, France

*E-mails: nicolas.lesniewska@univ-lorraine.fr, jerome.duval@univ-lorraine.fr

## Graphical Abstract

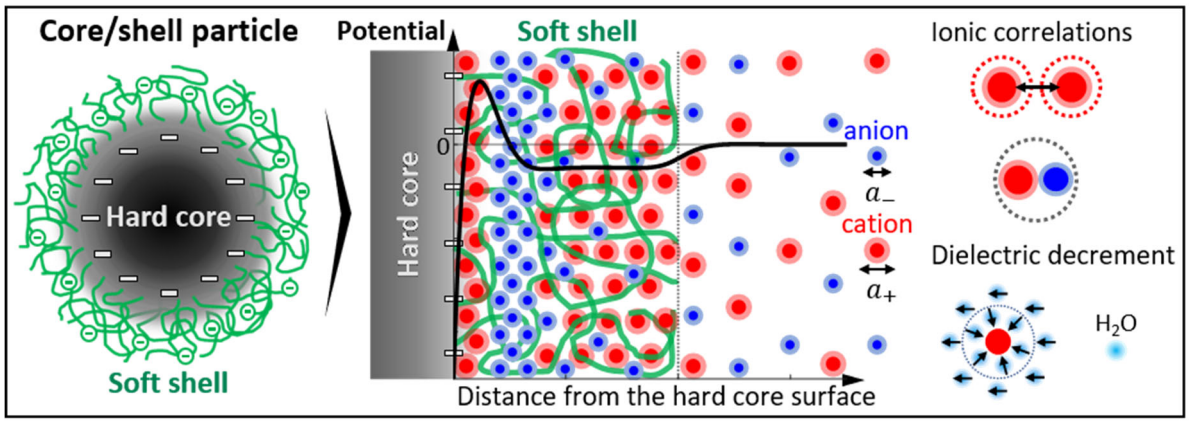

## Abstract

*Hypothesis*. Electrostatics of soft (ion-permeable) (bio)particles (e.g. microorganisms, core/shell colloids) in aqueous electrolytes is commonly formulated by the mean-field Poisson-Boltzmann theory and integration of the charge contributions from electrolyte ions and soft material. However, the effects connected to the size of the electrolyte ions and that of the structural charges carried by the particle, to dielectric decrement and ion-ion correlations on soft interface electrostatics have been so far considered at the margin, despite the limits of the Gouy theory for condensed and/or multivalent electrolytes. *Experiments.* Accordingly, we modify herein the Poisson-Boltzmann theory for core/shell (bio)interfaces to include the aforementioned molecular effects considered separately or concomitantly. The formalism is applicable for poorly to highly charged particles in the thin electric double layer regime and to unsymmetrical multivalent electrolytes. *Findings.* Computational examples of practical interests are discussed with emphasis on how each considered molecular effect or combination thereof affects the interfacial potential distribution depending on size and valence of cations and anions, size of particle charges, length scale of ionic correlations and shell-to-Debye layer thickness ratio. The origins of here-evidenced pseudo-harmonic potential profile and ion size-dependent screening of core/shell particle charges are detailed. In addition, the existence and magnitude of the Donnan potential when reached in the shell layer are shown to depend on the excluded volumes of the electrolyte ions.

**Keywords:** Soft interfaces, Electrostatics, Modified Poisson-Boltzmann theory, finite ion size, dielectric decrement, ion-ion correlations, soft particle heterogeneity.

## 1. Introduction.

Electric double layers (EDLs) play a central role in interface science and they are key components of surface electrohydrodynamics [1], particle electrodynamics [2], or colloid stability against aggregation in aqueous media [3,4]. Surface electrostatics is of further concern in numerous physicochemical processes underlying e.g. the reactivity of (nano)particles with respect to metals [5,6] and organic macromolecules [7,8], the (bioavai)lability of metal complexes at metal-accumulating biointerfaces [9,10], the ecotoxicology of metal oxide nanoparticles [11,12], the kinetics of electron transfer reactions at electrodic surfaces [13,14], or the thermodynamics of ionic surfactants [15,16].

Mechanistic assessment of the aforementioned processes is tied to a proper formulation of the spatial distribution for the electrostatic potential at the charged particle/electrolyte interface. In that respect, numerical and analytical solutions to the mean field Poisson-Boltzmann (MFPB) theory (cf. e.g. [17]) have long been elaborated for charged colloids that are impermeable to ions of the background electrolyte (so-called *hard interfaces*). Evaluation of MFPB formalism for such interfacial systems is now well documented over a large spectrum of electrostatic settings tackled or not within the Debye-Hückel approximation (cf. e.g. [18]). The scenarios explored so far include the analysis of effects associated with particle geometry and particle curvature to Debye layer thickness ratio [19], the influence of surface charge/potential magnitude [20], that of the ion valence and the electrolyte concentration [21] under conditions where EDLs of neighbouring particles are in interaction or electrically isolated [22]. The outcome of MFPB theory has been validated at qualitative and quantitative levels [23] from confrontation to simulations and experiments (e.g. electroosmosis [24], AC and DC electrophoresis [25], Atomic Force Microscopy (AFM) [26]), especially in dilute symmetrical electrolytes.

However, classical MFPB theory for hard interfaces suffers from several well-recognized limits [27]. Namely, it considers the electrolyte side of the particle/medium interface as an assembly of point-like ions, which comes to discard effects associated with finite ion size, ion-solvent and ion-ion interactions. Accordingly, there have been efforts in the literature to correct MFPB theory for finite ion size, dielectric decrement or ion-ion correlations [28,29], and evaluate experimentally their implications in several practical situations [30,31]. For the sake of illustration, ion condensation close to a charged surface explains why the use of the classical MFPB model may lead to misevaluation of particle surface charge density [32]. In addition, there is a large body of literature that pinpoints the importance of ionic correlations for sufficiently dense ionic clouds in the vicinity of charged surfaces (cf. e.g. [33] and references therein). Notably, ion-ion correlations at a charged interface may lead to the reversal of the surface charge due to charge overneutralization by the counterions then organized in a closed-packed layer adjacent to the surface, the thickness of that layer being dependent on ion size [29]. In line with experimental data, this phenomenon explains possible attractive electrostatics between hard surfaces

carrying charges of the same sign [34], or the reversal of the polarity of charged surfaces in water upon addition of multivalent ions [35]. The prediction of double-layer capacitance at electrode/solution interfaces under high applied voltage, the description of the specific adsorption of ions and the evaluation of the electrokinetic charge at hydrophobic or hydrophilic surfaces were further shown to be improved upon integration of spatially dependent dielectric permittivity in MFPB formalism for hard surfaces [36].

All above mean-field formulations of interfacial electrostatics refer to the case of hard interfaces/particles defined by a 2D charge distribution [37]. However it now accepted that this historical representation of interfaces does not apply to so-called soft colloids/interfaces that harbour 3D distributed structural charges [38], e.g. bacterial interfaces [39], viral particles [40], supported-polyelectrolyte layers and core/shell colloids [41], polymeric particles featuring a hairy surface layer [42], or particles like dendrimers [43], to quote only a few. Indeed, the defining electrostatic and electrokinetic properties of soft interfaces significantly differ from those of their hard counterparts, as evidenced by numerous experimental and theoretical reports invoking MFPB equation (uncorrected for molecular effects) with account of the contribution of 3D structural charges (cf. e.g. [44] and references therein). As an illustration, the electrophoretic mobility of soft particles with zwitterionic functionality (e.g. cationic core and anionic shell) was shown to change sign with varying the concentration of (dilute) *monovalent* electrolytes due to the respective contributions of the cationic and anionic structural charges to the potential at the shell/electrolyte interface depending on intraparticle Debye layer thickness [45], in line with AFM experiments [43].

Like for hard interfaces, the implementation of finite ion size, ion-ion correlations or dielectric decrement within MFPB theory applicable to soft particles/interfaces (**denoted hereafter as SMFPB**) is *a priori* required for a complete and comprehensive understanding of their electrostatic properties, especially for highly charged systems and/or multivalent electrolytes. However, to the best of our knowledge, reported corrections of SMFPB theory refer mainly to the implementation of finite ion size in symmetrical electrolytes for particulate systems whose soft layer thickness legitimates or not the applicability of Donnan electrostatic representation [46]. The presence of a charged rigid surface that supports this soft layer – a configuration that applies to numerous engineered soft (bio)interfaces and particles – is further generally ignored (cf. e.g. [47] and references therein).

In view of the above elements, we elaborate here an extension of the classical SMFPB model so as to describe the electrostatic potential distribution around an isolated core-shell particle in a multivalent electrolyte with full integration of the effects associated with finite ion size, dielectric decrement *and* ion-ion correlations. Numerical solutions of the so-modified SMFPB model are provided for different electrostatic descriptors pertaining to both the core and shell part of the soft particle under conditions where Donnan potential is reached or not within the soft particle layer [48].

Analytical equations defining the Donnan potential are further derived with the explicit account of finite ion size for both symmetrical and unsymmetrical electrolytes, and with the account of the size of the shell charges. The respective contributions of the charged (2D) core and (3D) shell particle components to the intertwined spatial distributions of counter/co-ions and electrostatic potential are critically analysed depending on the molecular effects (finite ions size, dielectric decrement and ionic correlations) that we consider separately or in combination. Overall, we address here the way in which each of these molecular effects contributes to the organisation of ions at a soft interface, from the very vicinity of the charged core to the shell layer and beyond. Of interest is the identification of the scenarios where modulations of the mean-field potential distribution caused by a given molecular effect are predominant, attenuated or dominated by variations of potential that result from another molecular process. The flexibility of the theory allows the treatment of the extremes of hard and fully porous particles (devoid of shell and core, respectively), as well as core/shell interfaces with zwitterionic functionality [45,49].

## 2. Theory.

### 2.1. Setting the stage.

In the following developments, we consider a spherical core/shell particle with radius $r_{\mathrm{p}} = r_{\mathrm{c}} + \delta$, where $r_{\mathrm{c}}$ and $\delta$ are the core radius and the shell layer thickness, respectively. In line with common assumption [38], the particle features here homogeneous distributions of charges along the core surface, and in the polar and azimuthal directions within the shell compartment (**Figure 1**). Accordingly, we adopt the radial coordinate system $r$ with the origin $r = 0$ positioned at the particle centre, and the introduction of inhomogeneous distribution of shell charges in the radial direction is possible (cf. discussion below). We define the dimensionless spatial variable $X$ by $X = \kappa\left(r - r_{\mathrm{c}}\right)$ where $\kappa^{-1}$ is the Debye layer thickness given by $\kappa^{-1} = 1/\sqrt{2F^2 I/\left(RT\varepsilon_0\varepsilon_{\mathrm{s}}\right)}$ with $\varepsilon_0$ the dielectric permittivity of the vacuum, $\varepsilon_{\mathrm{s}}$ the relative dielectric permittivity of the solvent (water), $R$ the gas constant, $T$ the absolute temperature, $F$ the Faraday number, and $I = \sum_{i=+,-} z_i^2 c_i^{\infty}/(2N_A)$ is the ionic strength of the solution (mol m$^{-3}$) that contains one type of cations and one type of anions with bulk number concentrations $c_+^{\infty}$ and $c_-^{\infty}$ (m$^{-3}$) and valences $z_+$ and $z_-$, respectively, and $N_A$ is the Avogadro number. Following Gupta et al. [50], we rewrite $c_+^{\infty}$ and $c_-^{\infty}$ in the form $c_+^{\infty} = z_- c_0$ and $c_-^{\infty} = z_+ c_0$ (which ensures bulk electroneutrality), so that $1/\kappa$ can be recast in the form

$$1/\kappa = 1/\sqrt{z_+ z_- \left(z_+ + z_-\right) e^2 c_0/\left(k_{\mathrm{B}} T \varepsilon_0 \varepsilon_{\mathrm{s}}\right)} \qquad (1)$$

with $k_B$ the Boltzmann constant and $e$ the elementary charge. The case of soft particles with radius $r_p$ verifying $\kappa r_p \gg 1$ (thin electric double layer regime) is addressed in this work. Such soft particles correspond to e.g. micro-sized biocolloids like bacteria or microalgae [51] or nanosized colloids (e.g. dendrimers or viruses [39,40,45]) dispersed in aqueous solutions with sufficiently high values of $I$. In turn, the electrostatic potential distribution at the particle/medium interface, denoted as $\psi(r)$, is governed by the Poisson-Boltzmann equation (modified or not for molecular effects) written in planar geometry [37,41]. We introduce below $y(r) = F\psi(r)/RT$ the dimensionless potential at the radial position $r$, and the corresponding dimensionless concentrations of cations and anions are denoted as $n_+(r) = c_+(r)/c_+^\infty$ and $n_-(r) = c_-(r)/c_-^\infty$, respectively, where $c_{+,-}(r)$ ($m^{-3}$) are the cations/anions densities at $r$. Following the representation of soft diffuse interfaces introduced by Duval and co-workers in the context of soft particle electrophoresis [52] and streaming potential/current of soft polymeric films [53], the density of structural charges $\rho_{fix}$ (C $m^{-3}$) in the shell may depend on the position $r$ within the shell particle component according to e.g.

$$\rho_{fix}(r)/\rho_0 = 2^{-1}\omega\left\{1 - \tanh\left[\alpha^{-1}\left(r - r_p\right)\right]\right\} \quad (2)$$

where $\alpha$ (m) is a spatial length scale that defines the degree of inhomogeneity (or diffuseness) for the density distribution of soft material that supports the structural charges of the shell. In Eq. (2), $\omega$ (dimensionless) is defined such that the total amount of structural charges within the soft particle shell is invariant with changing $\alpha$ and/or shell layer thickness $\delta$ [52]. We introduce accordingly the dimensionless amount $Q_0$ of shell structural charges defined by $Q_0 = 4\pi\int_{r_c}^{\infty}\left(|\rho_0|/e\right)f(r)r^2\mathrm{d}r$ where $f(r) = \rho_{fix}(r)/\rho_0$ is defined by Eq. (2). In the limit $\alpha/\delta \to 0$ (i.e. $\omega \to 1$), we have $\rho_{fix}(X) \to \rho_0$ with $\rho_0$ (C $m^{-3}$) the density of structural charges when homogeneously distributed within the particle shell volume. Equation (2) represents soft interfaces in a generic way that goes beyond the traditional assumption according to which shell charges are homogeneously distributed. Indeed, Eq. (2) can capture possible changes in the shell structure depending on solution composition, which translates into modifications of the parameter $\alpha$ and/or of the shell thickness $\delta$. In addition, the change of the *net* charge carried by the shell sites following e.g. adsorption of (multivalent) ions can be effectively modelled via a tuning of the smeared-out shell charge density $\rho_0$. Previous reports on electrokinetics of soft material showed that external stimuli such as electrolyte concentration [54] or pH [55] may induce swelling of the soft structures when repulsive electrostatics between adjacent shell charges becomes significant. The dramatic implications of such a swelling process (especially at low medium salinity) on e.g. the electrokinetic properties of soft particles and polymeric interfaces have been

successfully explained on a quantitative level with the account of charge and soft material inhomogeneity modelled on the basis of Eq. (2) [53,54,56]. Obviously, more advanced models have been developed to describe the interactions between e.g. multivalent electrolyte ions and shell components (and the possible formation of bridges between shell charges), and the resulting effects on the net charge and length of polyelectrolyte chains depending on e.g. the nature of the ionizable groups in the shell and chain elasticity (cf. e.g. [57] and references therein). The design of such models that include explicitly the interactions between shell charges and electrolyte ions on top of the here-targeted molecular effects may be doable for well-defined polyelectrolyte systems but remain extremely challenging for complex interfaces like e.g. bacteria that harbour complex soft surface structures like pili, proteins and/or fimbriae [1]. Reports have now largely evidenced that the electrophoretic mobility of soft particles like dendrimers, hairy latex particles, bacteria, microalgae or even viruses measured as a function of electrolyte concentration can be interpreted quantitatively by soft surface electrokinetic theory with implementation or not of soft structure heterogeneity via Eq. (2) depending on medium salinity and associated interface swelling properties [1,45].

Considering these elements, we here mostly report simulations for cases where shell charges are homogeneously distributed ( $\alpha / \delta \to 0$ ) so as to decipher properly the effects of ionic correlations, ion size, and dielectric decrement on soft interfacial electrostatics without contribution of a spatial gradient in shell charges. We further show, with a few illustrative computational examples, how the features defining potential distributions with account of molecular effects are modified upon introduction of such a spatial gradient that mark the changes of shell structure due to e.g. homogeneous swelling (increase of $\delta$ for $\alpha / \delta \to 0$ , and constant amount $Q_0$ of charges in the shell) or heterogeneous swelling (increase of both $\delta$ and $\alpha / \delta$ at constant $Q_0$ ). Finally, in line with the arguments detailed in [52], we stress that the sigmoid-like profile for soft material and shell charge density distribution adopted in Eq. (2) can be replaced by any other spatial function, may it be the result of independent theoretical simulations (cf. e.g. [58]) or experiments [59].

The core surface of the particle is hereafter defined by the surface potential $\psi_c$ with corresponding dimensionless potential $y_c$. Without loss of generality, the numerical code developed to solve the mean field Poisson-Boltzmann equation corrected for molecular effects can be straightforwardly adapted to tackle situations where electrostatics of particle core surface is defined by a surface charge density. We further assume that the amount of water in the soft layer is sufficiently high so that the dielectric permittivity in that layer equates that of the electrolyte solution, in line with the approximation often formulated in soft surface electrokinetic theories (cf. e.g. [60] and references therein). Finally, we introduce $a_{fix}$ the size of the shell sites that carry a charge, and $c_{fix}(r) = \left|\rho_{fix}(r)\right| / e$

(m$^{-3}$) is the number density of these sites in the shell. We denote as $c_{\mathrm{fix},0}$ the value of that density when charges are homogeneously distributed in the shell (case retrieved with $\alpha / \delta \to 0$ ).

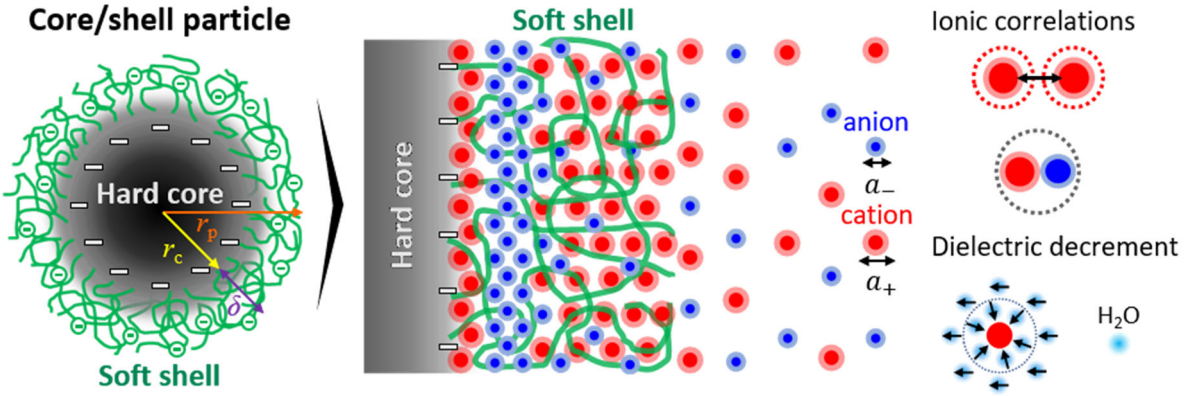


**Figure 1** . Schematics of a soft particle comprising a core and shell component, dispersed in an electrolyte where size and charge of cations (subscript '+') and anions (subscript '-') are given by $a_{+,-}$ and $z_{+,-}$, respectively. Electrostatics of the soft particle/electrolyte interface is detailed in this work with the account of finite ion size, ion-ion correlations, dielectric decrement and finite size of the shell charges.

The dielectric decrement is described as the effect of ion density at a given position $r$ on the solution dielectric permittivity that holds at that position. In detail, this decrement results from the combination of several defining properties of the ions. Namely, their size generates a so-called dielectric hole in the sense that water molecules are excluded from their body volumes. In addition, the solvent molecules in the hydration shell surrounding the electrolyte ions are strongly oriented [61] along the electrostatic field of each ion, which decreases their orientational polarizability and, in turn, increases effectively the dielectric decrement effect [62,63]. Overall, these modulations of the solution dielectric permittivity as mediated by electrolyte ion properties impact on the ion storage capacity of the medium and the interfacial potential distribution [50]. The dielectric decrement effect originating from the above interplay between dielectric permittivity at $r$ and corresponding ion densities can be written formally according to the following empirical relationship derived from experiments [64]

$$\varepsilon_{\mathrm{r}}(r) = \varepsilon_{\mathrm{s}} - \gamma_{+} c_{+}(r) - \gamma_{-} c_{-}(r) \tag{3}$$

where $\gamma_{+}$ and $\gamma_{-}$ (m$^3$) are the dielectric decrement coefficients (or hydration coefficients) pertaining to cations and anions, respectively [65], and their tabulated values depend on the ion considered [64]. Eq. (3) holds for solution ionic strengths less than 2 M, this limit being obtained from the critical value of $I$ marking significant deviations between linear predictions by Eq. (2) and experimental data [64].

We introduce below the *effective* radii $a_{+}$ and $a_{-}$ (m) of the cations and anions, respectively. The radii $a_{+,-}$, which are the central descriptors of ion-size effects, correspond to the minimal repulsion

distance between ions that carry charges of the same sign [66] and, accordingly, $a_{+,-}$ may exceed atomic radii. The quantities $a_+^3$ and $a_-^3$ define the excluded volume associated with each ion [46,66], which includes contribution from the hydration shell [67]. The mean volume fraction of ions in the bulk solution, denoted as $\nu$, is given by $\nu = \left(a_+/2 + a_-/2\right)^3 \left(c_+^\infty + c_-^\infty\right)$. Within the approximation of incompressible ionic volumes, the developments below hold for $\nu < 1$ and the formalism excludes the condensation (saturation) limit given by $\nu = 1$.

Last, we introduce the effective length scale $\ell_c$ for ion-ion electrostatic interactions in the electrolyte medium, and its dimensionless form $L_c$ is defined hereafter by $L_c = \kappa \ell_c$. $\ell_c$ corresponds to the ion-ion correlation length, which may be viewed as being to the ions what the standard electric Debye layer thickness $1/\kappa$ is for interacting particles [68]. However, this is where the comparison ends as $1/\kappa$ decreases with ion concentration and is independent of ion size, whereas $\ell_c$ inherently depends on the physical properties of the ions (including their size) and increases from dilute to concentrated ionic systems [69].

### 2.2. Soft Mean-Field Poisson-Boltzmann equation (SMFPB) corrected for molecular effects.

Below, we briefly describe the different steps leading to the correction of the SMFPB equation for the molecular effects defined in §2.1., i.e. the finite sizes of cations and anions, the dielectric decrement (Eq. (3)) and the ion-ion correlations. We start with the volumic free energy $G = U - TS$ (J m$^{-3}$) of the system schemed in **Figure 1** where $U$ (J m$^{-3}$) and $S$ (J K$^{-1}$ m$^{-3}$) are the internal energy and entropy per unit volume, respectively. The finite size considered for the ions generates a constrain on their spatial distribution at the charged particle/solution interface and it impacts the (mixing) entropy $S$ of the system. At equilibrium, $S$ can be formulated by the Boltzmann law, taking into account the different configurational microstates in terms of the occupancy of ions in the core, shell and electrolyte phases of the system displayed in **Figure 1**. For $a_+ \geq a_-$, the result reads as

$$S\left(c_+, c_-\right) = k_B \left[ \frac{1 - a_{fix}^3 c_{fix}}{a_+^3} \ln\left( \frac{1 - a_{fix}^3 c_{fix}}{1 - a_{fix}^3 c_{fix} - a_+^3 c_+} \right) - c_+ \ln\left( \frac{a_+^3 c_+}{1 - a_{fix}^3 c_{fix} - a_+^3 c_+} \right) - c_- \ln\left( \frac{a_-^3 c_-}{1 - a_{fix}^3 c_{fix} - a_+^3 c_+} \right) - \frac{1 - a_{fix}^3 c_{fix} - a_+^3 c_+ - a_-^3 c_-}{a_-^3} \ln\left( \frac{1 - a_{fix}^3 c_{fix} - a_+^3 c_+ - a_-^3 c_-}{1 - a_{fix}^3 c_{fix} - a_+^3 c_+} \right) \right] \quad (4)$$

where we have specified that $S\left(c_+, c_-\right)$ depends on the ion concentrations $c_{+,-}$. The case $a_- \geq a_+$ is simply retrieved from Eq. (4) by interchanging '+' with '−'. The expression for the internal energy $U$ per unit volume is further written

$$U = -\frac{\varepsilon_0 \varepsilon_r(r)}{2} \left[ \left( \frac{\partial \psi}{\partial r} \right)^2 + \ell_c^2 \left( \frac{\partial^2 \psi}{\partial r^2} \right)^2 \right] + z_+ e c_+ \psi - z_- e c_- \psi + \rho_0 f(r) \psi \quad (5)$$

where $e$ is the elementary charge, $f(r)=\rho_{\mathrm{fix}}(r)/\rho_0$ is the radial function defined by Eq. (2) and $\varepsilon_{\mathrm{r}}(r)$ is defined by Eq. (3). The three last terms in the right-hand side of Eq. (5) correspond to the electrostatic energies of the cations, anions and shell structural charges. The term $(\partial\psi/\partial r)^2$ stands for the Maxwell stress contribution while $\ell_{\mathrm{c}}^2\left(\partial^2\psi/\partial r^2\right)^2$ is the first-order correction of $U$ for the contribution of local ion electrostatics [70]. Using Eqs. (4) and (5), the expressions for the electrochemical potentials $\mu_+$ and $\mu_-$ of the cations and anions can be easily derived according to $\mu_{+,-}=\partial G/\partial c_{+,-}$. At equilibrium, for any position $r$ the quantities $\mu_+$ and $\mu_-$ verify the relationships $\mu_{+,-}=\mu_{+,-}^{\infty}$ where $\mu_{+,-}^{\infty}$ are the electrochemical potentials of cations and anions in bulk solution. In turn, we obtain for the dimensionless densities of cations and anions $n_{+,-}(r)=c_{+,-}(r)/c_{+,-}^{\infty}$

$$\begin{cases} n_+(r)=\dfrac{\mathrm{e}^{y_+(y)}}{g_{\mathrm{cc}}(y)} & \text{(a)} \\ n_-(r)=\dfrac{f_{\mathrm{cc}}(y)\mathrm{e}^{y_-(y)}}{g_{\mathrm{cc}}(y)} & \text{(b)} \end{cases} \tag{6}$$

where $y_+$ and $y_-$ depend on the dimensionless potential $y$ (and thus on the position $r$) according to

$$\begin{cases} y_+(y)=-z_+y+\dfrac{z_+z_-(z_++z_-)c_0}{2\varepsilon_{\mathrm{s}}}\dfrac{\partial\varepsilon_{\mathrm{r}}(X)}{\partial c_+}\left(\left(\dfrac{\partial y}{\partial X}\right)^2+L_{\mathrm{c}}^2\left(\dfrac{\partial^2 y}{\partial X^2}\right)^2\right) & \text{(a)} \\ y_-(y)=z_-y+\dfrac{z_+z_-(z_++z_-)c_0}{2\varepsilon_{\mathrm{s}}}\dfrac{\partial\varepsilon_{\mathrm{r}}(X)}{\partial c_-}\left(\left(\dfrac{\partial y}{\partial X}\right)^2+L_{\mathrm{c}}^2\left(\dfrac{\partial^2 y}{\partial X^2}\right)^2\right) & \text{(b)} \end{cases} \tag{7}$$

, which is written in terms of the dimensionless space variable $X=\kappa(r-r_{\mathrm{c}})$. The functions $f_{\mathrm{cc}}$ and $g_{\mathrm{cc}}$ involved in Eq. (6) further depend on $y$ (and therefore on $r$ or $X$) following

$$\begin{cases} f_{\mathrm{cc}}(y)=\left(1+\dfrac{a_-^3c_0z_+\left(\mathrm{e}^{y_-(y)}-1\right)}{1-a_+^3c_0z_-}\right)^{(a_+/a_-)^3-1} & \text{(a)} \\ g_{\mathrm{cc}}(y)=\dfrac{f_{\mathrm{cc}}(y)+a_+^3c_0z_-\left(\mathrm{e}^{y_+(y)}-f_{\mathrm{cc}}(y)\right)+a_-^3c_0z_+f_{\mathrm{cc}}(y)\left(\mathrm{e}^{y_-(y)}-1\right)}{1-a_{\mathrm{fix}}^3c_{\mathrm{fix}}} & \text{(b)} \end{cases} \tag{8}$$

Equations (6)-(8) generalize the result derived by Gupta and Stone [50] for hard interfaces to the situation of soft interfaces with account of the finite size of electrolyte ions and shell charges, dielectric decrement and ion-ion correlations. The $g_{\mathrm{cc}}$ function quantifies the decrease in ion concentrations at the position $r$ in the vicinity of the charged interface depending on the size of the ions, their valences and the electrostatic potential at $r$. The function $f_{\mathrm{cc}}$ reflects the asymmetry of the spatial distribution

of anions and cations caused by their differentiated sizes ( $f_{cc}=1$ for $a_+=a_-$ ), and this asymmetry is enhanced for $z_+\neq z_-$ .

In order to derive the electrostatic potential distribution, we minimize the free energy $G$ with respect to the electrostatic potential, $y(r)$ , to the electrical field, $-\partial y(r)/\partial r$ , and to the Laplacian of the potential, $\partial^2 y(r)/\partial r^2$ , using the Euler-Poisson equation written in terms of $X$ , i.e.

$$\sum_{k=0}^{2}(-1)^k\frac{\partial^k}{\partial X^k}\left[\frac{\partial G}{\partial\left(\partial^k y/\partial X^k\right)}\right]=0 \tag{9}$$

Combining Eq. (9) with Eqs. (4) and (5), we obtain

$$\frac{\partial}{\partial X}\left(\varepsilon_r(X)\frac{\partial y(X)}{\partial X}\right)-L_c^2\frac{\partial^2}{\partial X^2}\left(\varepsilon_r(X)\frac{\partial^2 y(X)}{\partial X^2}\right)=\varepsilon_s\left(\frac{n_-(X)-n_+(X)}{z_++z_-}-n_0 f(X)\right) \tag{10}$$

, where the dimensionless ion concentrations $n_{+,-}$ and the relative dielectric permittivity $\varepsilon_r$ both depend on the spatial position $X=\kappa(r-r_c)$ according to Eqs. (6)-(8) and Eq. (3), respectively, and $n_0$ is the dimensionless concentration (including sign) of structural charges defined by $n_0=\rho_0/(2IF)$ . Eq. (10) is an important result of this work as it stands for the SMFPB equation corrected for ion size, dielectric decrement *and* ion-ion correlations with account of the size of the shell charges. In §2.4, some limits of practical interest covered by Eq. (10) are analytically retrieved and discussed.

### 2.3. Boundary conditions of the SMFPB equation corrected for molecular effects.

The evaluation of the electrostatic potential $y(r)$ for any position $r$ at the particle core/shell/solution interfaces requires solving the fourth-order modified SMFPB equation given by Eq. (10) upon specifying relevant boundaries. Namely, at the particle core surface (i.e. $X=0$ ), we consider either an imposed core surface potential $\psi_c$ (V) or a charge density $\sigma_c$ (C m$^{-2}$), leading to the conditions $y(X=0)=y_c$ (selected in the developments below) or $\left(\varepsilon_r(X)\times\partial y(X)/\partial X\right)\big|_{X=0}=-\sigma_c F/(RT\varepsilon_0\kappa)$ (boundary (i)), respectively. As a result of this boundary, the correlations between ions and particle core surface are necessarily not accounted for. In turn, using Eq. (10) we obtain $L_c^2\partial\left(\varepsilon_r(X)\partial^2 y(X)/\partial X^2\right)/\partial X\big|_{X=0}=0$ (boundary (ii)), which reduces to $\partial^3 y(X)/\partial X^3\big|_{X=0}=0$ in the limit where dielectric decrement effects are ignored, in agreement with the formulation adopted in [29,32] for hard surfaces. Sufficiently far from the shell layer of the particle ( $X\to\infty$ ), the solution is electroneutral, i.e. $y(X\to\infty)=0$ (boundary (iii)) and, by extension, $\partial y(X)/\partial X\big|_{X\to\infty}=0$ (boundary (iv)).

### 2.4. Limiting cases covered by the SMFPB equation modified to include molecular effects.

***Case of hard interfaces*** **(** $n_0 = 0$ **).** In the limits where the shell layer is immaterial for the electrostatic potential distribution (i.e. $n_0 \to 0$, $a_{\text{fix}} \to 0$) and in the absence of either dielectric decrement effect ( $\varepsilon_{\text{r}}(X) \to \varepsilon_{\text{s}}$) and ion-ion correlations ( $L_{\text{c}} \to 0$), it is verified that Eq. (10) correctly reduces to the results derived by Gupta and Stone [50] for hard interfaces.

***Case of soft interfaces*** **(** $n_0 \neq 0$ **).** In the limits $L_{\text{c}} \to 0$, $a_{\text{fix}} \to 0$ and $a_{+,-} \to 0$ (i.e. shell charges and ions are point-like), and $\varepsilon_{\text{r}}(X) \to \varepsilon_{\text{s}}$, Eq. (10) reduces to the standard formulation of the mean field Poisson-Boltzmann equation for soft diffuse interfaces unmodified for molecular effects [48], i.e.

$$\frac{\partial^2 y(X)}{\partial X^2} = \frac{\mathrm{e}^{z_- y} - \mathrm{e}^{-z_+ y}}{z_+ + z_-} - n_0 f(X) \tag{11}$$

For homogeneous charge distribution in the particle shell ( $\alpha / \delta \to 0$ ), using the boundary conditions $y(X=0) = y_{\text{c}}$ and $y(X \to \infty) = 0$ (boundaries (i) and (iii) in §2.3), the solution of Eq. (11) in the Debye-Hückel approximation ( $y(X) \ll 1$ ) is given in Supplementary Material (**SM, section A**). The analytical solution of Eq. (11) with specifying core surface charge density instead of the core surface potential is further provided in **SM-A** for the sake of completeness. Under conditions where ion size, dielectric decrement and ionic correlations are ignored, we verified that the numerical solution of Eq. (10) correctly merges with these analytical solutions of Eq. (11) that are further in agreement with result from literature, cf. e.g. [48,53,54]. For a symmetrical electrolyte ( $a_+ = a_-$ and $z_+ = z_-$ ), homogeneous particle shell ( $\alpha / \delta \to 0$ ) and with neglect of dielectric decrement effects and ion-ion correlations ( $\varepsilon_{\text{r}}(X) \to \varepsilon_{\text{s}}$ and $L_{\text{c}} \to 0$ ), Eq. (10) further simplifies into the expressions given by Chanda and Das [46] and Barman and Bhattacharyya [71].

***Case of soft interfaces*** **(** $n_0 \neq 0$ **)** ***treated with modified SMFPB within Debye-Hückel approximation and with account of finite ion size.*** In the Debye-Hückel limit ( $y \ll 1$ ), accounting for the only finite ion size effects (i.e. $\varepsilon_{\text{r}}(X) \to \varepsilon_{\text{s}}$ and $L_{\text{c}} \to 0$ ), Eq. (10) becomes

$$\frac{\partial^2 y(X)}{\partial X^2} = \left[ \frac{\left(1 - a_-^3 c_0 z_-\right) z_+ + \left(1 - a_+^3 c_0 z_-\right) z_-}{\left(1 - a_+^3 c_0 z_-\right)\left(z_+ + z_-\right)} \right] y - n_0 f(X) \tag{12}$$

Making the analogy between the form of Eq. (12) and that obtained by linearization of the standard unmodified SMFPB equation we define

$$1/\kappa_{\text{mod}} = 1/\sqrt{\left( \frac{\left(1 - a_-^3 c_0 z_-\right) z_+ + \left(1 - a_+^3 c_0 z_-\right) z_-}{1 - a_+^3 c_0 z_-} \right) \frac{z_- z_+ e^2 c_0}{k_{\text{B}} T \varepsilon_0 \varepsilon_{\text{s}}}} \tag{13}$$

which holds for $a_+ \geq a_-$. The expression of $1/\kappa_{\mathrm{mod}}$ for $a_- \geq a_+$ is simply obtained by replacing the subscript '$+$' by '$-$' in Eq. (13). $1/\kappa_{\mathrm{mod}}$ is the equivalent of the classical screening Debye length $1/\kappa$ after effective correction for the finite sizes of the cations and anions, with the limiting case $1/\kappa \to 1/\kappa_{\mathrm{mod}}\big|_{a_{+,-}\to 0}$. We infer from Eq. (13) the equality $1/\kappa = 1/\kappa_{\mathrm{mod}}$ in the limit $a_- = a_+$, and the inequality $1/\kappa_{\mathrm{mod}} > 1/\kappa$ which holds regardless of the value of the ratio $a_-/a_+$. Stated differently, the sizes of the electrolyte ions contribute to decrease the screening of the electric double layer as compared to the standard situation where the ions are viewed as point-like charges. In addition, the analytical solution of the SMFPB equation corrected for ion sizes (Eq. (12)) is identical to that derived for $a_{+,-} \to 0$ (Eqs. (S3)-(S4) in **SM-A**) upon replacing $\kappa$ by $\kappa_{\mathrm{mod}}$ defined by Eq. (13).

***Case of soft interfaces*** **(** $n_0 \neq 0$ **)** ***defined by a Donnan phase.*** A constant electrostatic potential called the Donnan potential, denoted as $\psi_{\mathrm{D}}$ (with dimensionless form $y_{\mathrm{D}} = F\psi_{\mathrm{D}}/RT$), is achieved in the shell component of soft interfaces for cases where the shell layer thickness is much larger than the thickness of the operational Debye layer ($\kappa\delta \gg 1$) [48]. Replacing in Eq. (10) the terms $\partial^k y/\partial X^k$ with $k>1$ by 0 and further considering an homogeneous shell layer with point-like charges ($\alpha/\delta \to 0$ and $a_{\mathrm{fix}} \to 0$, respectively), it is found that $y_{\mathrm{D}}$ is determined by the transcendental equation (valid for $a_+ \geq a_-$)

$$0 = \frac{\mathrm{e}^{z_- y_{\mathrm{D}}} f_{\mathrm{cc}}\left(y_{\mathrm{D}}\right) - \mathrm{e}^{-z_+ y_{\mathrm{D}}}}{\left(z_- + z_+\right) g_{\mathrm{cc}}\left(y_{\mathrm{D}}\right)} - n_0 \tag{14}$$

where $f_{\mathrm{cc}}$ and $g_{\mathrm{cc}}$ are defined by Eq. (8). For a symmetrical electrolyte with $z_{+,-} = z$ and $a_{+,-} = 0$, it is straightforward to verify that the solution of Eq. (14) is given by $y_{\mathrm{D}} \equiv y_{\mathrm{D}}\big|_{\nu=0} = z^{-1}\sinh^{-1}\left(zn_0\right)$, which corresponds to the classical expression of the Donnan potential for a symmetrical electrolyte where charges of ions are point-like (i.e. $\nu = 0$) [38]. For $z_{+,-} = z$ and $a_{+,-} = a$, we demonstrate that the solution $y_{\mathrm{D}}$ of Eq. (14) can be written in the form (see details in **SM-B**)

$$y_{\mathrm{D}} = z^{-1}\left(\sinh^{-1}\left(\frac{\nu n_0 z}{\sqrt{1-\left(\nu n_0 z\right)^2}}\right) + \sinh^{-1}\left(\frac{\left(1-\nu\right)n_0 z}{\sqrt{1-\left(\nu n_0 z\right)^2}}\right)\right) \tag{15}$$

where $\nu = 2za^3c_0 < 1$ is a *natural measure of the nondiluteness* of the electrolyte (cf. §2.1) [62]. Eq. (15) correctly reduces to the standard result $y_{\mathrm{D}} = z^{-1}\sinh^{-1}\left(zn_0\right)$ applicable for $\nu = 0$. For $\nu \ll 1$, Eq. (15) further simplifies according to the following expression valid up to second order terms in $\nu$

$$y_D / y_D\big|_{\nu=0} = 1 + \frac{\left[1 + n_0 z + (n_0 z)^2\right] e^{-z y_D|_{(\nu=0)}} - 1}{y_D|_{(\nu=0)}\, e^{-z y_D|_{(\nu=0)}}} \frac{n_0 z}{1 + (n_0 z)^2} \nu \qquad (16)$$

which highlights the connection between $y_D$ at any $\nu \ll 1$ and $y_D$ at $\nu = 0$. It can be shown that Eq. (15) is defined on the condition that $\nu$ and $n_0$ verify the inequality $1 - \nu |n_0| z > 0$ (we recall that $n_0 = \rho_0 / (2IF)$ includes the sign of the volume charge density $\rho_0$). This condition, together with the condition $\kappa\delta \gg 1$, defines the scenarios where a Donnan potential is achieved in the shell phase. From a physical point of view, the inequality $1 - \nu |n_0| z > 0$ states that the accumulation of electrolyte ions in the shell layer, as required to neutralize the structural charges therein and build a Donnan potential, may be limited by the excluded volume of the electrolyte ions, especially so if the shell carries a high amount of charges (high value of $|\rho_0|$ or $|n_0|$). In turn, it becomes impossible to build up a Donnan potential in a shell layer carrying a density of charges that exceeds a threshold value of $|n_0|$ defined by $1/(\nu z)$. This important property is illustrated in **Figure 2a** where we draw the domains of existence of $y_D$ in the 2D representation $(n_0; \nu)$. **Figure 2b** further evidences an increase of the ratio $y_D / y_D|_{\nu=0}$ with increasing $\nu$ for selected values of $|n_0| z$, which reflects a decrease of the screening of the shell charge with increasing ion size. For a fixed value of $\nu$, the larger is $|n_0| z$, the more significant becomes this decrease of the shell charge screening and the larger is $y_D / y_D|_{\nu=0}$.

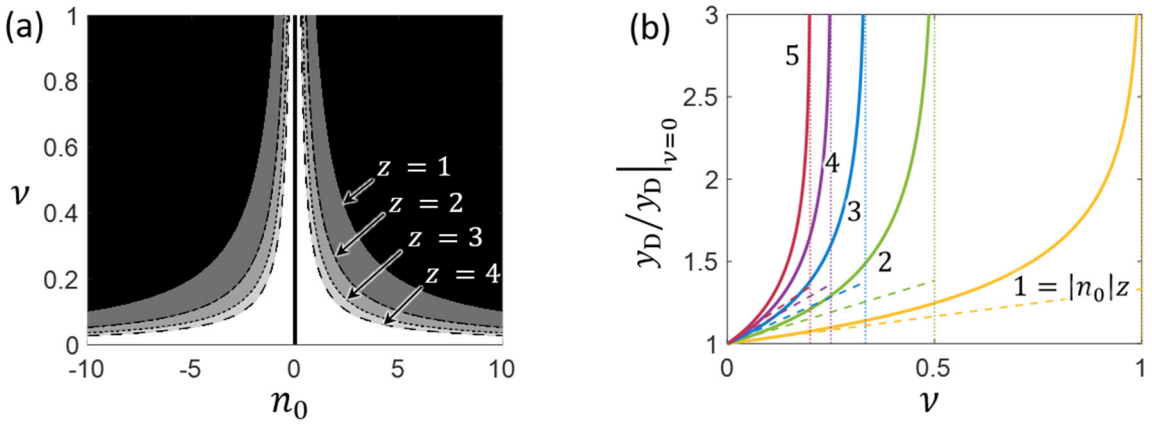


**Figure 2**. **(a)** Domains of existence of a Donnan potential (bright areas under the plain and dotted lines) for a symmetrical electrolyte containing cations and anions of similar size and valence, $a$ and $z$, respectively. The frontiers between bright and black areas are given for different values of $z$, and they are defined by $1 - \nu |n_0| z = 0$, with $n_0 = \rho_0 / (2IF)$ and $\nu$ is the parameter reflecting the nondiluteness of the electrolyte. **(b)** Dependence of $y_D / y_D|_{\nu=0}$ on $\nu$ at different values of $|n_0| z$ (indicated) for $z = 1$. The vertical short-dotted lines correspond to the limit $\nu = 1/(|n_0| z)$ and the long-dotted lines are predictions from Eq. (16). The results are given for a homogeneous charge distribution in the shell layer ($\alpha / \delta \to 0$) with neglecting the steric effect associated to the size of the shell charges (i.e. $a_{fix}^3 c_{fix,0} \to 0$).

The physics that holds beyond the condition marking a critical ion accumulation in the soft layer, i.e. $a_{-sign(n_0)}^3 \times c_{-sign(n_0)}\left(X < \kappa\delta\right) = 1$, is not tackled by Eqs. (6)-(8) and (10). We anticipate that a non-zero electric field remains inside ions-saturated soft layers, which prevents the establishment of a homogeneous (Donnan) potential in the shell layer under such conditions.

### 2.5. Numerical solution of the corrected SMFPB equation and validation.

For prescribed values of the parameters defining the geometry and electrostatic descriptors of the soft interface schemed in **Figure 1** (i.e. $a_{+,-}$; $z_{+,-}$; $\gamma_{+,-}$; $L_c$; $c_0$; $\kappa\delta$; $y_c$ and $n_0$), Eqs. (6)-(8) and (10) were solved by means of the numerical package COLSYS which approximates the solution $y(r)$ through spline-collocation at Gaussian nodes and selects the mesh subdivision following an auto-adaptative strategy [72]. For that purpose, a FORTRAN program was developed and it is available upon request. The robustness and flexibility of our program as well as the validity of the solution obtained for the SMFPB equation corrected for molecular effects (ion size, dielectric decrement and/or ion-ion correlations) were addressed successfully upon comparison with analytical results obtained in the limiting scenarios described in §2.4. In particular, the results reported by Gupta and Stone [50] for hard interfaces were all correctly reproduced by our numerical scheme in the limit $\kappa\delta \to 0$ and $n_0 \to 0$. In addition, the electrostatic potential profiles given by Chanda et al. [46] for soft interfaces in a symmetrical electrolyte with account of ion size were also correctly retrieved.

## 3. Results and discussion.

In the developments that follow, we report illustrative computational examples to analyse how size of electrolyte ions and shell charges, dielectric decrement and ion-ion correlations impact on the potential distribution $y(r)$ in situations where these molecular effects are considered separately (§3.1, §3.2 and §3.3) or in combination (§3.4). In turn, the analysis allows to appreciate the spatial scales over which each effect significantly modulates the potential profile depending on electrolyte concentration, distribution and density of structural charges in the particle shell, dimension of the shell and potential at the particle core surface. Last, we emphasize that the range of values selected for the relevant dimensionless parameters describing ion size (or steric) effects ($a_{+,-}^3 c_0$), dielectric decrement ($\gamma_{+,-} c_0$) and ion-ion correlations ($L_c = \kappa \ell_c$) are in agreement with those defined elsewhere for cases of practical interest [64,73,74].

### 3.1. Ion-size effects.

In this section, the way in which the potential profile $y(r)$ is modulated by ion size in the absence of dielectric decrement and ion-ion correlations (i.e. $\gamma_{+,-}c_0 \to 0$ and $L_c \to 0$, respectively) is investigated as a function of the key structural and charge features of the shell, i.e. for different values of the (dimensionless) shell thickness $\kappa\delta$ (**Figure 3a**), structural charge density $n_0$ (**Figure 3b**) and interface diffuseness (or heterogeneity parameter) $\alpha / \delta$ (**Figure 3c**), all other parameters being fixed. **Figure 3d** further reports modifications of the potential distribution with varying both $\kappa\delta$ and $\alpha / \delta$, a situation that is relevant for systems that undergo heterogeneous swelling under condition of constant total amount of charges in the shell (cf. §2.1). For that purpose, numerical solutions of the modified SMFPB equation (§2.5) derived for a symmetrical monovalent electrolyte defined by $a_{+,-}^3 c_0 = 0.2$ are systematically compared to the corresponding predictions by the unmodified SMFPB equation (Eq. (11)). Qualitatively, the characteristics of the potential profile $y(r)$ evaluated under the conditions of **Figure 3** (i.e. $sign(y_c \times n_0) < 0$) conform to those expected for zwitterionic particles, with the observation of a sign reversal for the potential across the core/shell interface. Under the conditions of **Figure 3** (symmetrical electrolyte), the potential $y(r)$ uncorrected for ion size is systematically lower in absolute value compared to that derived from modified SMFPB equation. This result is explained by the steric effect and related excluded volume of the ions, which leads to a significant reduction in the amount of (counter-)ions accumulated in the particle shell so that, in turn, the electric double layer screening is highest for point-like charges, i.e. within unmodified SMFPB model (cf. §2.4 and **Figure S1** in **SM-C**). This finding is particularly clear for the scenario where a Donnan phase is established ($\kappa\delta \gg 1$) (**Figure 3a**) and/or for increasing (absolute) values of the charge density $|n_0|$ in the shell (**Figure 3b**), these two situations being those where particle/solution interface electrostatics is dominated by $n_0$ rather than $y_c$. In situations where structural charge density is not homogeneous in the shell, i.e. for values of $\alpha / \delta$ that deviate significantly from 0 (**Figures 3c-d**), the distribution profile selected for the charge density in the shell (Eq. (2) and inset **Figure 3c**) impact on the shape of the potential distribution along the lines discussed in [52]. The ensuing modification of the potential profiles are observed regardless of the magnitude of the ion steric effects. **Figure 3c** unravels that an increase in the diffuseness $\alpha / \delta$ of the soft particle component (with a resulting potential profile that extends further to the solution side of the interface) leads to a significant decrease of the impact of the ion size on the potential distribution for $X \le \kappa\delta$ because of the corresponding decrease therein of the charge density (see inset), which supports the results of **Figure 3b**. **Figure 3d** features how the potential profiles change with increasing $\kappa\delta$ and interface diffuseness at fixed total amount of structural charges (with a resulting decrease of the shell charge density in the bulk of the shell, see

inset in **Figure 3d**). The results basically combine the features highlighted in **Figures 3a,b,c** where the impacts of $\kappa\delta$, $\alpha/\delta$ and $n_0$ on excluded ion-volume effects and related interface electrostatics were examined separately. The changes of potential associated to variations in the density of structural charges (cf. **Figure 3b** for an homogeneous shell) and in shell thickness (**Figure 3a**) are most significantly reflected in the potential profiles displayed in **Figure 3d**. As an intermediate conclusion, **Figure 3** evidences that the discrepancy between potential predictions by modified and unmodified SMFPB equations is largest as the shell charge density and/or shell thickness increases, and this trend is mitigated by the interface diffuseness/heterogeneity of the shell structure and related modulations of the shell charge density. The soft nature of the particle/solution interface thus enhances and extends in space the impact of ion size on resulting interfacial electrostatics.

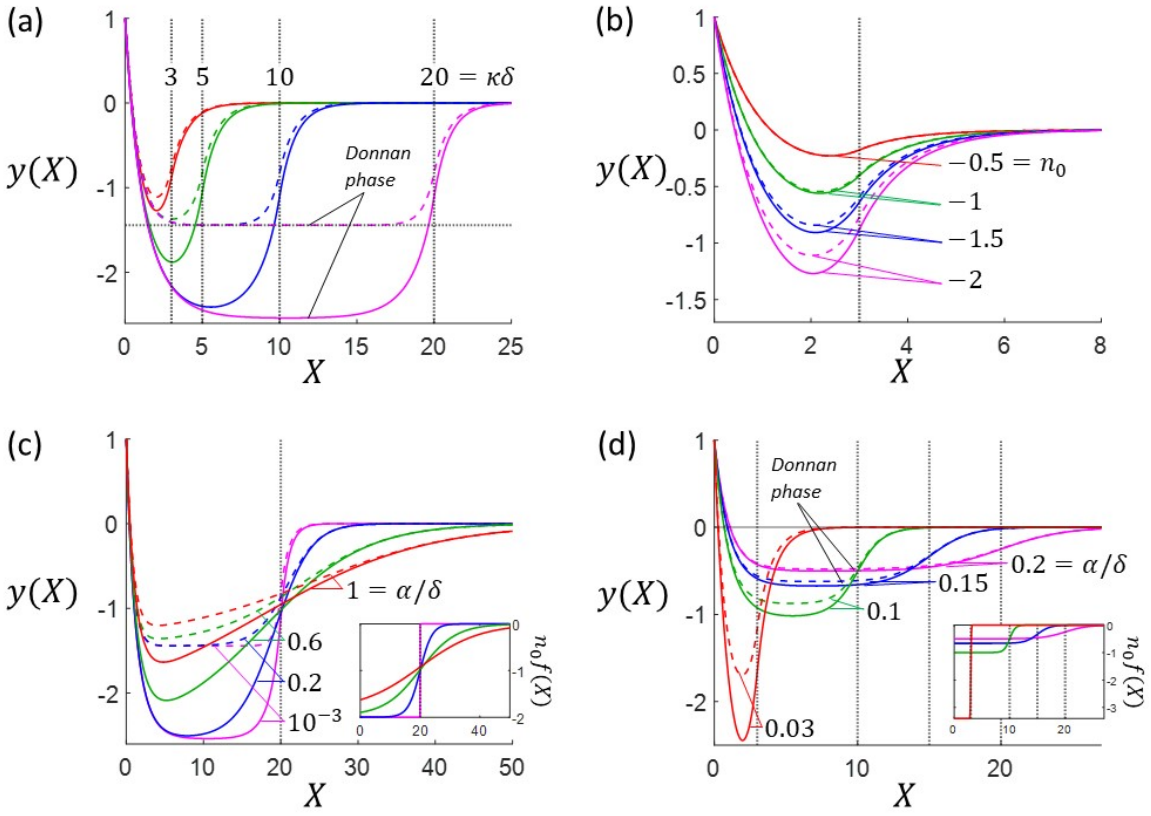


**Figure 3.** Dimensionless electrostatic potential distribution $y(X)$ at a soft particle/solution interface (colored solid curves) with core surface potential $y_c = 1$, in contact with a symmetrical electrolyte ($z_{+,-} = 1$, $a_{+,-} = a$), as a function of the dimensionless **(a)** soft layer thickness $\kappa\delta$ (indicated) for $n_0 = -2$ and homogeneous distribution of structural charges in the shell ($\alpha/\delta \to 0$), **(b)** density of shell structural charges (indicated) for $\alpha/\delta \to 0$ and $\kappa\delta = 3$, **(c)** interface diffuseness (or heterogeneity parameter) $\alpha/\delta$ (indicated) for $\kappa\delta = 20$ and $Q_0 = 8.70\times10^7$, and **(d)** shell thickness $\kappa\delta$ ($\kappa\delta = 3$, 10, 15 and 20 corresponding to red, green, blue and purple curves, respectively) and interface diffuseness $\alpha/\delta$ (indicated) under the condition of constant total amount of shell charges $Q_0 = 2.17\times10^7$. Insets in **(c)** and **(d)** show the dimensionless density distributions of structural shell charges $n_0 f(X)$ that correspond to the reported potential profiles. In **(a-d)**, the position of the

shell/solution interface is marked by the vertical black dotted lines. Colored dotted curves refer to predictions from SMFPB equation unmodified for steric effects (Eq. (11)). Other model parameters: $a_{\mathrm{fix}}^3 c_{\mathrm{fix},0} \to 0$, $a_{+,-}^3 c_0 = 0.2$, $\gamma_{+,-} c_0 \to 0$, $L_{\mathrm{c}} \to 0$, $I = 10$ mM.

**Figures 4a and 4b** illustrate the impacts of steric effect associated to the size $a_{\mathrm{fix}}$ of the shell charges on the potential distribution and corresponding ion density profiles, respectively. Reported simulations further account for the finite size of the electrolyte ions under conditions where a Donnan potential is established. **Figure 4b** shows that the increase of the excluded volume of shell charges causes a decrease in the densities of counter- and co-ions, which results in a decrease of the screening of the particle charge by the electrolyte ions **Figure 4a** and in an increase (in absolute value) of the potential. As intuitively expected, within the first order formulation of the mixed entropy of the system with respect to the term $a_{\mathrm{fix}}^3$ (Eq. (4)), an increase of the effective size of the shell charges at fixed $a_{+,-} = a$ has qualitatively the same implications for the potential distribution as those caused by an increase of the electrolyte ion size at fixed $a_{\mathrm{fix}}$. Given this result, we detail below scenarios where the only steric effects connected to finite ion size are considered in addition to ionic correlations and/or dielectric decrement.

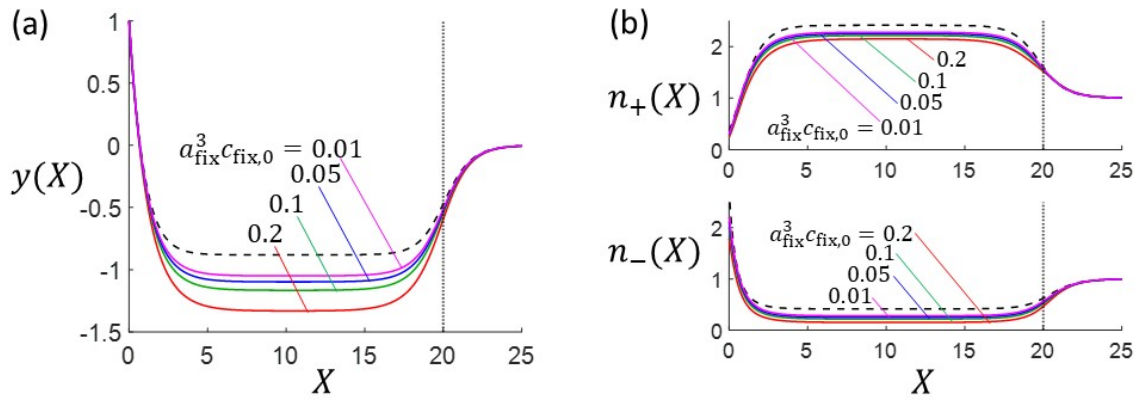


**Figure 4. (a)** Dimensionless electrostatic potential distribution $y(X)$ and **(b)** dimensionless cations and anions densities, $n_+(X)$ and $n_-(X)$, respectively, at a soft particle/solution interface (colored solid curves) for a core surface potential $y_{\mathrm{c}} = 1$ and a dimensionless structural charge density $n_0 = -1$, in contact with a symmetrical electrolyte ($z_{+,-} = 1, a_{+,-} = a$), as a function of the dimensionless size $a_{\mathrm{fix}}^3 c_{\mathrm{fix},0}$ of the shell charges (indicated). The vertical dotted lines mark the positioning of the surface layer, and the dotted curves refer to predictions from unmodified SMFPB equation (Eq. (11)). Other model parameters: $\alpha / \delta \to 0$, $a_{+,-}^3 c_0 = 0.2$, $\gamma_{+,-} c_0 \to 0$, $L_{\mathrm{c}} \to 0$, $I = 10$ mM.

**Figure 5** unravels the way in which the differentiated sizes of the electrolyte cations and anions affect the potential distribution $y(r)$. In **Figure 5a**, the size of the anions (which represent the coions

under the selected conditions $y_c < 0$ and $n_0 < 0$) is fixed. With decreasing the size of the cations (the counterions in the example) from $a_-$ to $a_-/2$, the potential $y$ (in absolute value) decreases for any position $r$. This finding is the result of their increased accumulation in the shell layer (and of the associated increase in shell charge screening) due to their decreasing excluded volume. Interestingly, predictions from unmodified SMFPB equations either underestimate or overestimate the outcomes of modified SMFPB model depending on the ratio $a_+/a_-$. This non-monotonous evolution of the deviation between $y(r)$ distributions formulated by modified and unmodified SMFPB equations is explained by a size-mediated balance between intra-shell accumulation of cations and anions (**Figure S2 in SM-C**). In detail, the extent of cation accumulation in the shell basically coincides with that from standard theory at sufficiently low $a_+/a_-$ (**Figure S2a**). In contrast, the exclusion of the anions from the (negatively charged) shell layer is reduced with decreasing $a_+/a_-$ in response to the increased accumulation of the cations and accompanied decrease in $|y(r)|$, and the level of anions depletion for $a_+/a_- \ll 1$ remains higher than the one predicted by the unmodified SMFPB due their finite size (**Figure S2a**). **Figure 5b** depicts a situation analogue to that of **Figure 5a** except for the sign of $n_0$ ($n_0 > 0$). **Figure 5b** evidences a decrease of $|y(r)|$ with decreasing cation size for the same reason as that invoked in **Figure 5a**. The new feature is that this effect has limited implications on the magnitude of the potential (see inset **Figure 5b**) because the cations serve here as coions for the positively charged shell layer and the size of the counterions (the anions, predominant in the shell, **Figure S2b**) is kept constant in the simulations. Overall, it is the size of the counterions within the shell layer that most significantly determines how steric effects modulate the potential distribution compared to the standard mean-field situation.

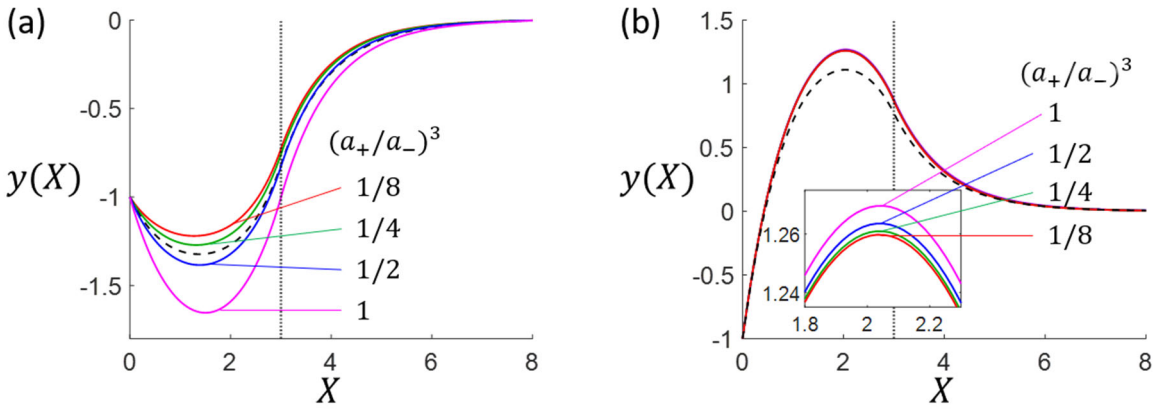


**Figure 5.** Dimensionless electrostatic potential distribution $y(X)$ at a soft particle/solution interface (colored solid curves) with imposed core surface potential $y_c = -1$, in contact with an electrolyte defined by $z_{+,-} = 1$ and different cation/anion volume ratios $(a_+/a_-)^3$ (indicated) for $\kappa\delta = 3$ with **(a)** $n_0 = -2$ and **(b)** $n_0 = 2$. The vertical dotted lines mark the positioning of the surface layer, and the

black dotted curve refers to predictions from unmodified SMFPB equation (Eq. (11)). Other model parameters: $\alpha/\delta \to 0$, $a_{\mathrm{fix}}^3 c_{\mathrm{fix},0} \to 0$, $a_-^3 c_0 = 0.2$, $\gamma_{+,-} c_0 \to 0$, $L_c \to 0$, $I = 10$ mM.

In **Figure 6a**, we analyse the dependence of the potential distribution $y(r)$ (at constant solution ionic strength) for electrolytes defined by similar size of cations and anions and distinct valence $z_+$ and $z_-$ under Donnan electrostatic condition in the shell layer (with $n_0 < 0$). Setting $z_-$ to unity, $|y(r)|$ decreases with increasing $z_+$ (which holds for both modified and unmodified SMFPB formulations of electrostatics), and $|y(r)|$ obtained from the modified SMFPB equation is slightly larger than that derived from its unmodified counterpart. These findings correlate with an increase (decrease) of the particle charge screening with increasing valence (size, respectively) of the counterions (here the cations). **Figure S3a** reports the (dimensionless) ion concentration profiles $n_{+,-}(r)$ (Eqs. (6)-(8)) corresponding to the conditions selected for **Figure 6a**. As expected, the unmodified SMFPB predicts a continuous increase of $n_-(r) = \mathrm{e}^{z_- y(r)}$ in the shell for increasing values of $z_+$ and a resulting decrease in $|y(r)|$ with $y(r) < 0$. Similar conclusion applies to $n_+(r) = \mathrm{e}^{-z_+ y(r)}$ because the increase of $z_+$ outweighs the resulting decrease in $|y(r)|$. This trend is basically maintained for $n_+(r)$ derived from modified SMFPB, but not for $n_-(r)$ that gradually reaches a saturation plateau value in the shell for $z_+ > 1$. Manifestly, the contribution of highly charged cations (the counterions in the example) outweighs that of the anions to such an extent that accumulation of the latter in the shell becomes limited as compared to that derived from standard mean field estimation. The features discussed in **Figure 6a** for $n_0 < 0$ slightly differ from those derived for the $n_0 > 0$ case where anions are the counterions in the Donnan phase (**Figure 6b**). Indeed, increasing the valence of cations leads to their significant exclusion from the here positively charged shell, to an increased accumulation of anions (**Figure S3b**) that is combined to an increase in $y(r)(>0)$. This finding is observed for the modified and unmodified SMFPB equations, in line with Eq. (11) applied to the Donnan phase for increasing values of $z_+$ at fixed $z_-$. Most remarkably, the increase in $y(r)$ predicted by unmodified SMFPB is here less significant than that derived with modified SMFPB despite of quasi-similar $n_{+,-}(r)$ profiles in the shell (**Figure S3b**). In **Figure 6b** (as in **Figure 6a**), the ionic strength is kept constant so that, in turn, an increase in $z_+$ at fixed $z_-$ is associated with a decrease in the bulk concentration of anions (defined by $c_-^\infty = c_0 z_+ = 2N_A I / \left[ z_- (z_+ + z_-) \right]$, cf. §2.1) and, therefore, with a decrease of $c_0$. At fixed $a_{+,-}^3 c_0$, the effective radius of the cations and anions thus increases with $z_+$. Consequently, under the conditions of **Figure 6b**, the screening of the positive shell charges by the anions decreases (cf. **Figure 5**) and the potential in the shell increases with $z_+$. We further observe that $n_-(r)$ in the shell reaches a saturation

value at sufficiently high $z_+$ (**Figure S3b**), which corresponds to a critical nondiluteness of the intra-shell electrolyte (§2.4) defined by $a_-^3 c_0 z_+ \times n_- \left(X < \kappa\delta\right) \to 1$ for $n_0 > 0$, expression that directly follows from Eq. (4). For such a condition that approaches the condensation limit, the Donnan potential largely exceeds the values estimated by the unmodified mean field equation, as illustrated in **Figure 2b** for symmetrical electrolytes. Overall, **Figure 6** highlights the importance of both the valence and the finite size of the ions in governing the electrostatics of soft particles, which constitutes an extension of the results reported for hard interfaces [50].

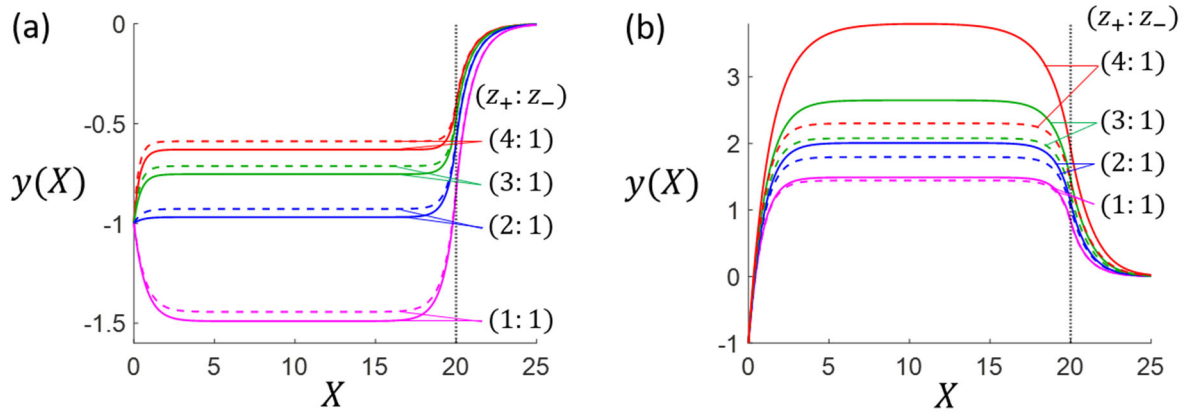


**Figure 6.** Dimensionless electrostatic potential distribution $y(X)$ at a soft particle/solution interface (colored solid curves) with core surface potential $y_c = -1$, in contact with an electrolyte defined by $z_- = 1$ and different cation valence $z_+$ (indicated) for $\kappa\delta = 20$ with **(a)** $n_0 = -2$ and **(b)** $n_0 = 2$. The vertical dotted lines mark the positioning of the surface layer, and the colored dotted curves refer to predictions from unmodified SMFPB equation (Eq. (11)). Other model parameters: $\alpha / \delta \to 0$, $a_{\text{fix}}^3 c_{\text{fix},0} \to 0$, $a_{+,-}^3 c_0 = 0.02$, $\gamma_{+,-} c_0 \to 0$, $L_c \to 0$, $I = 10$ mM.

### 3.2. Dielectric decrement.

In the developments that follow, the impacts of the dielectric decrement on the interfacial potential distribution $y(r)$ is investigated on the basis of Eqs. (3), (6)-(8) and (10) for homogeneous shell charge distribution ($\alpha / \delta \to 0$) in the limits $a_{+,-} \to 0$ and $L_c \to 0$ that cancel the effects of ion size and ion-ion correlations, respectively.

**Figure 7a** displays the potential profile $y(r)$ for negatively charged particle core and shell components under Donnan condition for different values of the hydration coefficients $\gamma_+$ and $\gamma_-$ (Eq. (3)) taken identical for the sake of simplicity ($\gamma_{+,-} = \gamma$). As expected, increasing $\gamma c_0$ leads to a decrease in $\varepsilon_r$ (or an increasing dielectric decrement, cf. Eq. (3) and **Figure S4a**) and therefore to an enhanced screening of the particle charge, which in turn generates a slight decrease of $|y(r)|$ (**Figure 7a** and inset therein). This decrease is most pronounced in the spatial region of the interface corresponding to highest electric fields and concentrations of counterions (cf. Eq. (3)), i.e. in the close vicinity of the

particle core surface (cf. inset in **Figure 7a**). This correlation between dielectric decrement effects and electric field is evidenced from straightforward inspection of Eq. (10) that involves products between $\varepsilon_r$ and either the first or second order derivatives of the potential with respect to space variable. Obviously, the value of the Donnan potential is not affected by the dielectric decrement as the Donnan phase is defined by a zero-electric field condition therein. It is further verified that predictions from unmodified and modified SMFPB equations correctly merge in the limit $\gamma c_0 \to 0$.

**Figure 7b** shows the impact of dielectric decrement on the interfacial potential distribution for a potential at the particle core surface (anionic) that is significantly higher (in absolute value) than that adopted in **Figure 7a** ( $y_c = -5$ in **Figure 7b**) and in situation where conditions for the establishment of a Donnan phase within the soft (cationic) layer are not met. In **Figure 7b** the increase of the particle charge screening when increasing $\gamma c_0$ (or decreasing $\varepsilon_r$) is now reflected by the decrease in $|y(r)|$ for only specific positions of the shell (cf. inset in **Figure 7b** for $1.85 \le X \le 1.9$). This decrease in $|y(r)|$ is preceded by an opposite effect for positions that are closer to the hard surface (cf. inset in **Figure 7b** for $X \ll 1$), which relates to the existence of a plateau value reached by the density of accumulated counterions (cations in the example) close to the particle core surface at sufficiently large $\gamma c_0$ (**Figure S5** in **SM-C**). Within the close-packed phase of the electrolyte at the very vicinity of the charged surface, values of $\varepsilon_r(X \to 0)$ are indeed so low (**Figure S4b** in **SM-C**) that the (counter-)ions storage capacity of the interface is reduced. The region close to the hard surface then behaves as a molecular capacitor, a feature discussed by Gupta and Stone [50] for the case of hard interfaces. Any further decrease in $\varepsilon_r$ (or increase in $\gamma c_0$) then leads to a more gradual decay of the potential from the core surface to the shell layer, in line with the results given in **Figure 7b** (compare e.g. blue and red curves in the inset for $X \ll 1$) and in qualitative agreement with the first order derivation given in [50] for the electric field at the surface of a hard particle as a function of $\gamma c_0$.

Comparison between results discussed in **Figures 3-7** indicates that changes of the potential distribution $y(r)$ due to dielectric decrement are far less significant as compared to those originating from ion size. In addition, dielectric decrement effects are most pronounced for highly charged systems and/or high solution ionic strengths. Unlike ion steric effects that propagate all through the shell component of soft particles, dielectric decrement is immaterial in the shell layer as long as a Donnan potential is established therein.

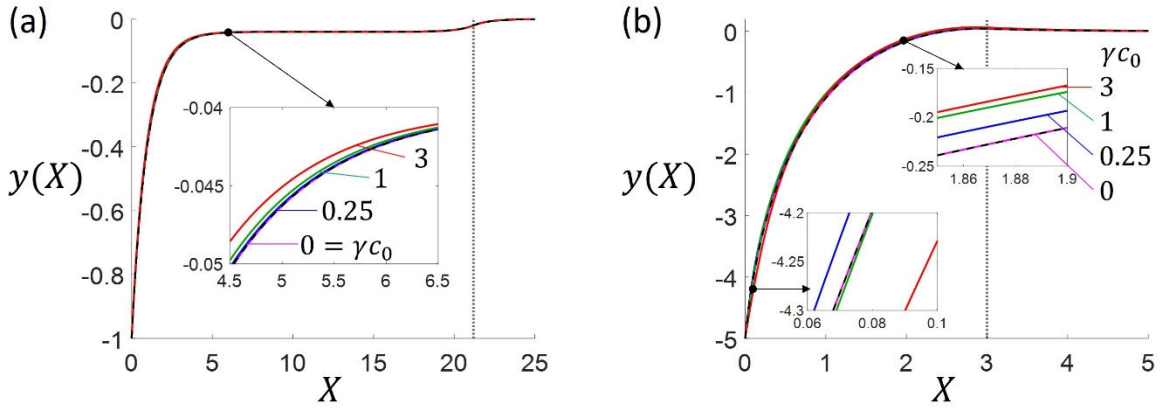


**Figure 7**. Dimensionless electrostatic potential distribution $y(X)$ at a soft particle/solution interface (colored solid curves) with core surface potential **(a)** $y_c = -1$, **(b)** $y_c = -5$, in contact with an electrolyte defined by $z_{+,-} = 1$ and different hydration coefficient of the ions $\gamma = \gamma_{+,-}$ (indicated) for **(a)** $\kappa\delta = 21.2$ and $n_0 = -0.04$, **(b)** $\kappa\delta = 3$ and $n_0 = -0.5$. The vertical dotted lines mark the positioning of the surface layer, and the black dotted curve refer to predictions from unmodified SMFPB equation (Eq. (11)). Other model parameters: $\alpha / \delta \to 0$, $a_{\text{fix}}^3 c_{\text{fix},0} \to 0$, $a_{+,-}^3 c_0 \to 0$, $L_c \to 0$, $I = 500$ mM.

565

566 **3.3. Ion-ion correlation effects.**

567 Like dielectric decrement effects, ion-ion correlations are formally associated to high-order
568 derivatives of the potential with respect to space (cf. Eq. (10)). Accordingly, within the conditions that
569 legitimate the use of the modified SMFPB equation, ion-ion correlations do not impact on $y(r)$ in the
570 spatial region of the particle/solution interface where the electrical field is 0, which includes the
571 Donnan phase when relevant (§2.4). In the case of hard interfaces, it is known that ion-ion correlations
572 lead to an inversion of the sign of the potential distribution [74]. This well-documented phenomenon
573 is explained by an overscreening of the particle surface charge by a dense layer of counterions, which
574 in turn generates locally a potential with sign opposite to that of the particle surface potential [29].
575 Following the procedure adopted in the previous sections, the contribution of ion-ion correlations to
576 the potential distribution at a soft interface is captured below by discarding dielectric decrement
577 effects ($\gamma_{+,-} c_0 \to 0$), and entropic effects due to sizes of ions and shell charges ($a_{+,-} \to 0$, $a_{\text{fix}} \to 0$),
578 keeping in mind that ionic correlations inherently encompass steric repulsion between ions [32].

579 **Figure 8a** shows how ion-ion correlations modulate the interfacial potential distribution in the
580 situation where a Donnan phase is established in a shell carrying (positive) charges of sign opposite to
581 that of the charges at the core surface. For values of the correlation length close to or larger than the
582 Debye length (i.e. $L_c \geq 1$), we observe 3 local extrema in the potential distribution, with these extrema
583 being positioned at the interface between particle core and shell, and at each side of the shell/solution
584 interface (the extrema are identified by the symbol * in **Figure 8a** for clarity). **Figure 8a** further

evidences a crossover (marked by the symbol ⊥) of the potential distributions evaluated for different values of $L_c$ at positions close to the particle core surface (i.e. $1 < X < 5$). Upon increase of $L_c$, the magnitude and width of the oscillation peak near the core surface clearly increase, its position is shifted slightly away from the particle core surface, and a shallow local minimum that follows that peak can even be detected for values of $L_c$ above unity (cf. inset **Figure 8a** for $7 < X < 17$). Obviously, for sufficiently high $L_c$ at fixed shell thickness, the Donnan situation is no longer established as the potential can then significantly fluctuate in the shell compartment, with a resulting electric field that deviates from non-zero value therein. At the shell/solution interface (i.e. at $X = \kappa\delta$ marked by a vertical dotted line in **Figure 8a**), increasing values of $L_c$ leads to a reduction of the electric field. This effect, here detailed for an homogeneous soft interface (*i.e.* $\alpha / \delta \to 0$ in Eq. (2)), is qualitatively similar to that discussed in [52] for soft heterogeneous interfaces characterized by increasing $\alpha / \delta$ in the absence of ion-ion correlation ( $L_c \to 0$, also cf. **Figures 3c-d**). The overall pseudo-oscillatory transition of the electrostatic potential observed from the particle core surface to the electrolyte medium is further reflected in the spatial distributions of the ionic density $n_{+,-}(r)$, namely by a local overshoot and depletion of counterions and coions in the shell, respectively (**Figure 8b**). In **Figure 8c**, we analyse how the potential distribution is modified by ion-ion correlations upon increasing the (absolute) value of the core surface potential $|y_c|$, under conditions where pseudo-oscillations in the potential profile are most pronounced ( $L_c = 2$ in **Figure 8a**), all other parameters being fixed. Unlike in **Figure 8a** where we considered a particle core and a shell layer that carried charges of opposite sign (which generates a reversal of the potential regardless of $L_c$), a potential reversal is evidenced in **Figure 8c** for a core and shell components that both carry anionic charges. This potential reversal originating from ion-ion correlations is most significant at largest $|y_c|$. Indeed, such high values of $|y_c|$ generate – at fixed charge density $n_0$ of structural charges in the shell – high electric fields at the particle core surface, which in turn drives an overscreening of the particle core surface charge due to excess of counterions accumulation at $X \to 0$ as compared to predictions from unmodified SMFPB equation [29] (**Figure 8d** and inset therein). This leads to an excess of coions in the next layer, thus resulting in oscillations of the charge density of counterions and coions until electroneutrality is reached in layers sufficiently far from the particle (**Figure 8d**). As the selected ion-ion correlation length is higher than the classical screening Debye layer thickness ( $L_c = 2$ in **Figure 8c-d**), the potential generated by the layer of accumulated cations at the particle core surface decays over a spatial region that goes beyond the classical screening Debye layer domain.

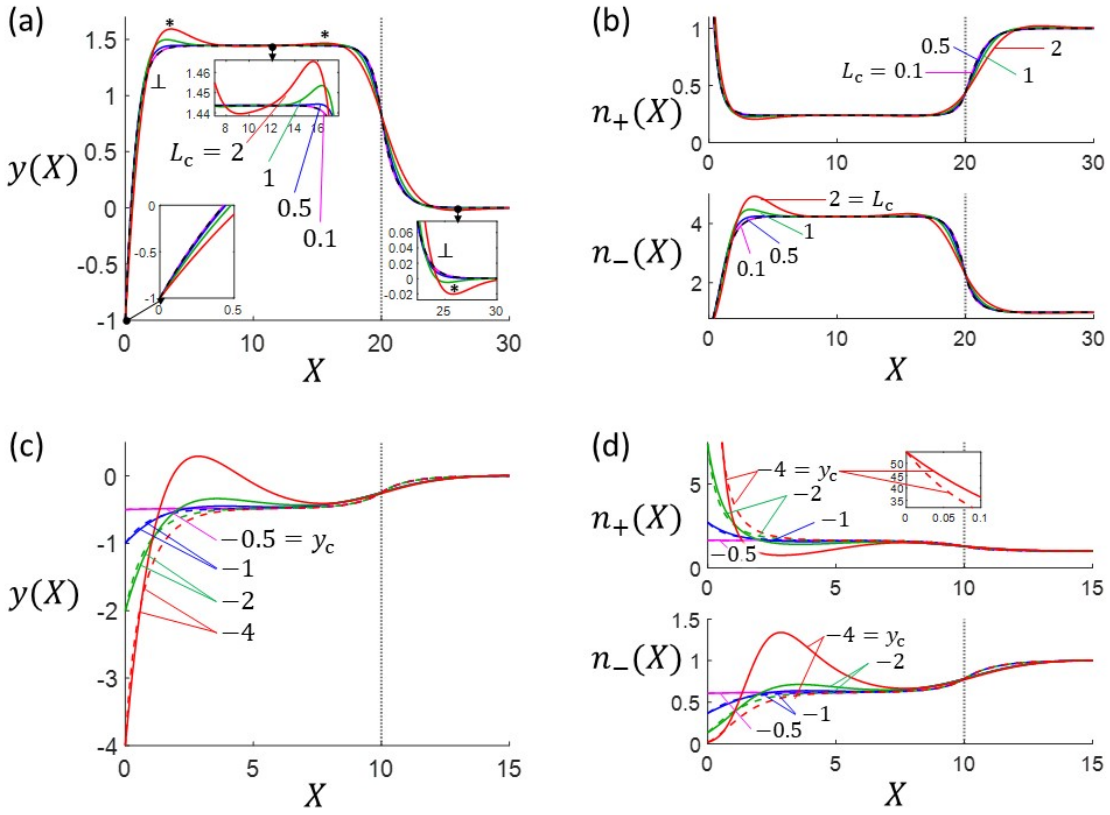


**Figure 8. (a)** and **(c)** Dimensionless electrostatic potential distribution $y(X)$, **(b)** and **(d)** corresponding dimensionless cations and anions densities, $n_+(X)$ and $n_-(X)$, respectively, at a soft particle/solution interface (colored solid curves) in contact with an electrolyte defined by $z_{+,-} = 1$. In **(a)** and **(b)**, $y(X)$ and $n_{+,-}(X)$ are given for $y_c = -1$ and different values of the dimensionless correlation length $L_c$ (indicated) for $\kappa\delta = 20$ and $n_0 = 2$. The symbols * and ⊥ feature positions where local extrema of $y(X)$ and a cross-over between $y(X)$ curves generated at different $L_c$ are observed, respectively. In **(a)**, the insets zoom some characteristic features of $y(X)$ depending on $L_c$. In **(c)** and **(d)**, $y(X)$ and $n_{+,-}(X)$ are reported for different values of $y_c$ (indicated), and $L_c = 2$, $\kappa\delta = 10$ and $n_0 = -0.5$. The inset in **(d)** zooms the excess of accumulated counterions (cations) at $X \to 0$ for $y_c = -4$. The vertical dotted lines mark the positioning of the surface layer, and the dotted curves refer to predictions from unmodified SMFPB equation (Eq. (11)). Other model parameters: $\alpha / \delta \to 0$, $a_{fix}^3 c_{fix,0} \to 0$, $a_{+,-}^3 c_0 \to 0$, $\gamma_{+,-} c_0 \to 0$, $I = 10$ mM.

### 3.4. Combined effects of ion size, dielectric decrement and ion-ion correlations.

In this section, we briefly analyse how ion size, dielectric decrement and ion-ion correlations considered *concomitantly* determine the electrostatic potential distribution at the core/shell/solution interfaces in comparison to predictions from unmodified SMFPB equation. In the first selected example (**Figure 9a**), the effective radii $a_{+,-}$ are considered as descriptors of the spatial range of ion-ion electrostatic interactions and we adopt accordingly $a_{+,-} \sim \ell_c$ (= 0.8 nm) in agreement with the choice made in other studies [73]. Under the conditions selected in **Figure 9a** (particle core surface and shell

layer are negatively charged, homogenous shell charges distribution and $\kappa\delta = 10$), the effects due to finite ion size and ion-ion correlations dominate those associated with dielectric decrement whose variation over space is reported in **Figure S6a (SM-C)**. In agreement with **Figure 8**, ion-ion correlations generate a reversal of the electric potential and a layering of ion densities (**Figure S6b** in **SM-C**) while ion steric effects decrease the screening of the particle charge as compared to the screening level expected from unmodified SMFPB equation. **Figure 9a** shows that the joint consideration of the three molecular effects of interest leads to an interfacial potential profile that features the remarkable properties generated by ion steric effects and ion-ion correlations considered separately, i.e. a decrease of the particle charge screening and the apparition of a local potential extremum (with a reversal of the sign of the potential) as compared to standard mean-field predictions.

Finally, **Figure 9b** simulates a scenario in line with the existence of marked pseudo-oscillations in the potential profile for a anionic core/shell particle (with account of excluded volume of electrolyte ions) and focuses on the way these oscillations are modified when changing the structure of the shell component via increasing shell thickness ($\kappa\delta$) and interface diffuseness ($\alpha / \delta$) at constant total amount of shell charges (cf. **Figure 3d**). **Figure 9b** clearly shows that the increase of $\kappa\delta$ and $\alpha / \delta$ leads to an increase in the magnitude of the maximum of the peak potential essentially because the resulting lowering of the density (in magnitude) of structural charges deep inside the shell leads to higher electric fields close to the core surface, which magnifies the ion-ion correlations effects (cf. the analogous trend observed in **Figure 8c**). The features of the potential profiles beyond the region where pseudo-oscillations exist, are further similar to those discussed in **Figure 3d**. The density profiles of anions and cations corresponding to the potential distributions displayed in **Figure 9b** are given in **Figure S7** (**SM-C**). Briefly, with increasing $\kappa\delta$ and $\alpha / \delta$ the layering of the counterions (cations) is gradually shifted to higher positions $X$ and the associated amplitude of the peaks decreases. This is connected to the increased accumulation of coions (anions) in the shell that follows a reduction in the magnitude of the (negative) charge density close to the core surface when increasing $\kappa\delta$ and $\alpha / \delta$ at constant $Q_0$ (cf. inset **Figure 9b**). The peak position of the coions remains essentially independent of $\kappa\delta$ and $\alpha / \delta$, and $n_{-}(X)$ closely follows the variations of $y(X)$ when changing shell thickness and interface diffuseness parameter. Overall, **Figure 9b** illustrates the intricate relationships between magnitude of operational molecular effects and the changes of the shell structure and resulting descriptors of shell electrostatic properties (cf. inset **Figure 9b**).

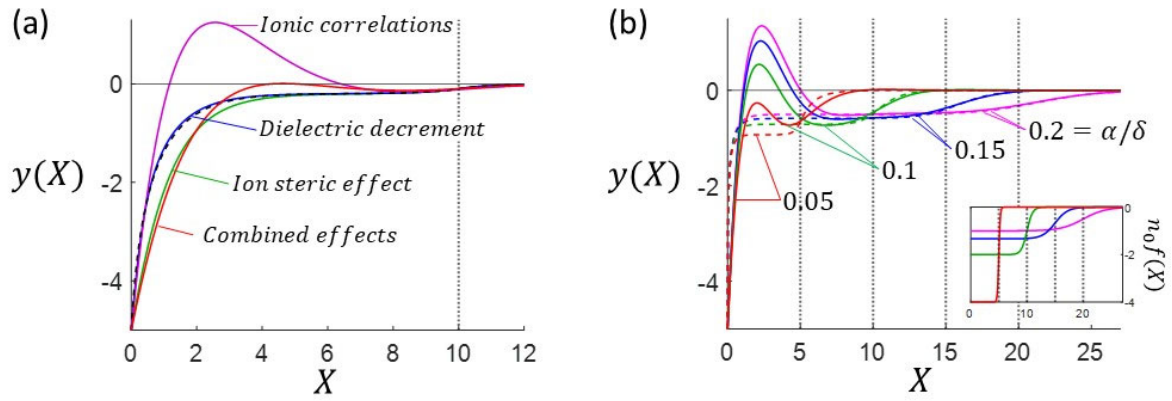


**Figure 9. (a)** Dimensionless electrostatic potential distribution $y(X)$ (colored solid curves) for $\kappa\delta = 10$, $n_0 = -0.2$ and $y_c = -5$, $z_{+,-} = 1$. The figure reports the results derived from corrected SMFPB equation (Eq. (10)) with $a_{+,-}^3 c_0 = 0.2$, $\gamma_{+,-} c_0 = 3$ and $L_c = 2$. The contributions of each molecular effect taken separately (indicated) to the potential profile is displayed. Ion steric effects are given for $a_{+,-}^3 c_0 = 0.2$ and $(\gamma_{+,-} c_0, L_c) \to (0,0)$, dielectric decrement for $\gamma_{+,-} c_0 = 3$ and $(a_{+,-}^3 c_0, L_c) \to (0,0)$, ion-ion correlations for $L_c = 2$ and $(a_{+,-}^3 c_0, \gamma_{+,-} c_0) \to (0,0)$. The vertical dotted lines mark the positioning of the surface layer, and the black dotted curve represents predictions from unmodified SMFPB equation. Other model parameters adopted: $\alpha / \delta \to 0$ (homogeneous charge distribution in the shell layer), $a_{fix}^3 c_{fix,0} \to 0$, $I = 500$ mM. **(b)** Dimensionless electrostatic potential distribution $y(X)$ (colored solid curves) with $y_c = -5$, in contact with a multivalent electrolyte defined by $z_+ = 3$, $z_- = 1$, $a_+^3 c_0 = 0.01$, $a_-^3 c_0 = 0.05$, $\gamma_{+,-} c_0 = 0.1$ and $L_c = 2$, as a function of the interface diffuseness parameter $\alpha / \delta$ and shell thickness $\kappa\delta$ for a constant total amount of shell charges $Q_0 = 1.35 \times 10^8$ (dimensionless). The position of the shell/solution interface is marked by the vertical black dotted lines. Colored dotted curves refer to predictions from unmodified SMFPB equation (Eq. (11)). Other model parameters: $a_{fix}^3 c_{fix,0} \to 0$, $I = 100$ mM. The inset in **(d)** shows the dimensionless density distributions of shell charges, $n_0 f(X)$, that correspond to the reported potential profiles.

## 4. Conclusions and perspectives.

In this study, we report a modification of the mean-field Poisson Boltzmann equation applicable to soft interfaces and soft particles so as to account for ion size, dielectric decrement and ion-ion correlations. Paradigms of (bio)systems for which the model is relevant include microalgae, yeast, bacteria, latex particles to quote a few [1,75,76]. The proposed model allows the evaluation of the electrostatic potential distribution at a particle core/shell/solution interface in contact with an asymmetrical and multivalent electrolyte, assuming that the double layer thickness is small compared to the particle dimension and further ignoring lateral contributions to core surface electrostatics. The dielectric decrement and the ion-ion correlations are shown to mainly affect the potential distribution at the core/shell and shell/solution interfaces, respectively, while the explicit account of excluded volumes of electrolyte ions basically leads to a reduction in the screening of the charges originating

from the particle core surface and shell layer. We further show that the finite size of the structural charges in the shell leads to an additional reduction of particle charge screening by electrolyte ions as compared to the situation where shell charges are treated as point-like objects.

As expected from modified MFPB models addressing the historical case of hard surfaces [27,32,50], the potential distributions derived with use of a modified SMFPB equation that concomitantly includes all three molecular effects of interest, deviate significantly from those obtained with unmodified SMFPB equation, with respect to both magnitude and sign, and also in terms of the positioning of the potential reversal for soft particles with zwitterionic functionality. We further show how the existence of a Donnan potential in the shell layer is conditioned by the magnitude of the volume charge density that is operational therein *and* by the nondiluteness of the electrolyte which is mediated by ion steric effects. This condition adds to the conventional constraint that shell dimension must significantly exceed the Debye layer thickness for a Donnan phase with constant potential to be generated in the particle shell layer.

Within the framework of this modelling study, possible inhomogeneity of the shell can be taken into account, and the spatial distribution of the structural charges carried by the shell particle component is fixed regardless of the electrolyte composition. The work thus avoids the complex modelling of possible impacts of the electrolyte ions on the very structure of the shell with e.g. resulting shell swelling/shrinking. The latter processes are instead effectively represented by ad hoc variations of the shell thickness and the interface heterogeneity parameter, in line with common practice for the analysis of the electrokinetic response of soft heterogeneous surfaces [52–55,75]. Obviously, a deeper understanding of the electrostatics of well-defined polyelectrolyte interfaces [55] may benefit from advanced implementation of local ion-shell correlations, but the design of such models for more complex soft biological particles remains a challenging task [30]. In this work, we evidence how heterogeneous distributions of structural charges in the shell impact the electrostatic potential profile. Namely, this heterogeneity, reflected by a gradual expansion of the charged shell towards the outer electrolyte solution, is accompanied by a decrease of the charge density in the bulk shell under the condition of constant total amount of shell charges, as relevant for e.g. swollen particles. In turn, this leads to an increase of the electric field at the particle core surface and to a decrease of the magnitude of the potential in the shell, with a resulting extension of the interfacial domain where ion-ion correlations are operational and a decrease of ion steric effects in the shell. This translates into a shift in space of the peak potential maxima and minima that characterize the pseudo-oscillatory potential distribution at the interface, these oscillations being a signature of significant ion-ion correlations.

Application of this work includes the evaluation of the electrokinetic properties of soft interfaces (e.g. streaming potential/current and DC electrophoresis) with account of ion size and ionic

correlations. Such an evaluation would require the coupling of our modified SMFPB formulation of soft interfacial electrostatics with tangential flow hydrodynamics driven by e.g. applied pressure gradient or electric field. Last, the here-reported electrostatic formalism can help in the formulation of non-DLVO electrostatic interaction forces exerted between a soft particle and a neighbouring charged colloid or surface in a complex aqueous environment, which will be the subject of a forthcoming contribution. The formalism provides experimentalists an extended theoretical arsenal to interpret experimental data beyond the standard mean-field formulation of soft surface electrostatics (SSE) that ignores effects on potential caused by the size/valence of electrolyte ions, size and distribution of the structural charges located in the shell, dielectric decrement and ion-ion correlations. Simulations given in this work evidence clearly how conventional potential profiles at soft interfaces under conditions legitimating or not the Donnan electrostatic representation, are specifically modified by the aforementioned effects taken separately or in combination. The underlying guidelines for identifying the significance of one effect compared to another is expected to be relevant to address e.g. particle-particle interactions or electric double layer properties that cannot be understood from standard SSE concepts, especially in dispersing media of complex ionic composition and/or high salinity. Such situations are common in environmental and biological settings, e.g. cell-cell aggregation, drug delivery by soft particles, metal complexation by natural or synthetic particulate ligands, or soft particle interactions in confined media. Suitable techniques to capture molecular electrostatic processes include atomic force microscopy for the measurement of particle interfacial properties and interactions between colloids [77], high energy X-ray reflectivity for addressing electric double layer composition with Angstrom resolution [78], fluidics and electrokinetics in soft nanochannels [79] or scattering techniques to monitor aggregation kinetics in complex media [80], to quote a few. To the best of our knowledge, systematic measurements to address the electric double layer properties of soft interfaces and/or their interactions under conditions (identified in this work) where the above molecular electrostatic effects are at stake are still lacking in literature.

**CRediT authorship contribution statement.**

**Nicolas Lesniewska**: Methodology, Software, Formal analysis, Validation, Investigation, Writing - original draft. **Audrey Beaussart**: Investigation, Writing - review & editing, Supervision. **Jérôme F.L. Duval**: Conceptualization, Methodology, Software, Formal analysis, Investigation, Writing - review & editing, Supervision.

**Declaration of Competing Interest.** The authors declare that they have no known competing financial interests or personal relationships that could have appeared to influence the work reported in this paper.

**Supplementary material.** Supplementary data to this article can be found online at https://doi.org/XXX.

## Glossary of symbols.

### Latin symbols

$a_+$, $a_-$ effective radii of cations and anions (m), respectively

$c_+(r)$, $c_-(r)$ densities of cations and anions ($m^{-3}$) defined by $c_+^\infty = c_0 z_-$ and $c_-^\infty = c_0 z_+$

$c_{\mathrm{fix}}(r)$ density of shell charges at position *r*, defined by $c_{\mathrm{fix}}(r) = |\rho_0| f(r)/e$

$c_{\mathrm{fix},0}$ defined by $c_{\mathrm{fix},0} = c_{\mathrm{fix}}(r = r_{\mathrm{c}})$

$I$ solution ionic strength (mol $m^{-3}$)

$\ell_{\mathrm{c}}$ correlation length (m), $L_{\mathrm{c}} = \kappa \ell_{\mathrm{c}}$ (dimensionless)

$n_0$ dimensionless density of structural charges in the shell

$n_+(r)$, $n_-(r)$ dimensionless densities of cations and anions at position $r$, respectively

$r$ radial coordinate (m)

$r_{\mathrm{c}}$ hard particle core radius (m)

$r_{\mathrm{p}}$ soft particle radius (m), with $r_{\mathrm{p}} = r_{\mathrm{c}} + \delta$

$Q_0$ total amount of structural charges in the shell defined by $Q_0 = 4\pi \int_{r_{\mathrm{c}}}^{\infty} \left(|\rho_0|/e\right) f(r) r^2 \mathrm{d}r$

$X$ dimensionless space variable defined by $X = \kappa(r - r_{\mathrm{c}})$

$y(r)$ dimensionless potential at position $r$

$y_{\mathrm{c}}$ dimensionless core surface potential

$y_{\mathrm{D}}$ dimensionless Donnan potential

$z_+$, $z_-$ unsigned valences of cations and anions, respectively

### Greek symbols

$\alpha$ spatial length scale defining the distribution the structural shell charges (m)

$\delta$ soft layer thickness (m)

$\varepsilon_0$ dielectric permittivity of vacuum ($F\ m^{-1}$)

$\varepsilon_{\mathrm{r}}(r)$ relative permittivity of the electrolyte solution at position $r$

$\varepsilon_{\mathrm{s}}$ relative permittivity of the solvent (water)

$\gamma_+$, $\gamma_-$ hydration coefficients of cations and anions ($m^3$)

$1/\kappa$ Debye length (m)

$\nu$ measure of the nondiluteness of the electrolyte, $\nu = \left(a_+/2 + a_-/2\right)^3 (c_+^\infty + c_-^\infty)$

$\rho_0$ density of structural charges homogeneously distributed within the shell ($C\ m^{-3}$)

$\rho_{\mathrm{fix}}(r)$ density of structural charges at position $r$ ($C\ m^{-3}$) as defined by Eq. (2)

770 $\psi(r)$ electrostatic potential at position $r$ (V)

771 $\sigma_c$ core surface charge density (C m$^{-2}$), $\sum_c = \sigma_c e / (k_B T \varepsilon_0 \varepsilon_s \kappa)$ (dimensionless)

## References


[1] J.F.L. Duval, F. Gaboriaud, Progress in electrohydrodynamics of soft microbial particle interphases, Curr Opin Colloid Interface Sci. 15 (2010) 184–195. https://doi.org/10.1016/j.cocis.2009.12.002.

[2] B. Podolsky, P. Schwed, Review of a generalized electrodynamics, Rev. Mod. Phys. 20 (1948) 40–50.

[3] E.J.W. Verwey, On the repulsive forces between charged colloid particles and on the theory of slow coagulation and stability of lyophobe sols, Trans. Faraday Soc. 35 (1940) 203–215.

[4] J. Liu, Y. Gao, D. Cao, L. Zhang, Z. Guo, Nanoparticle dispersion and aggregation in polymer nanocomposites: Insights from molecular dynamics simulation, Langmuir. 27 (2011) 7926–7933. https://doi.org/10.1021/la201073m.

[5] J.F.L. Duval, Chemodynamics of metal ion complexation by charged nanoparticles a dimensionless rationale for soft, core–shell and hard particle types, Phys. Chem. Chem. Phys. 19 (2017) 11802–11815. https://doi.org/10.1039/C7CP01750B.

[6] E. Iskrenova-Tchoukova, A.G. Kalinichev, R. James Kirkpatrick, Metal cation complexation with natural organic matter in aqueous solutions: Molecular dynamics simulations and potentials of mean force, Langmuir. 26 (2020) 15909–15919. https://doi.org/10.1021/la102535n.

[7] C.L. Tiller, C.R. O'melia, Natural organic matter and colloidal stability: models and measurements, Colloids Surf. A Physicochem. Eng. Asp. 73 (1993) 89–102. https://doi.org/10.1016/0927-7757(93)80009-4.

[8] J.P. Pinheiro, E. Rotureau, J.F.L. Duval, Addressing the electrostatic component of protons binding to aquatic nanoparticles beyond the Non-Ideal Competitive Adsorption (NICA)-Donnan level: theory and application to analysis of proton titration data for humic matter, J. Colloid Interface Sci. 583 (2021) 642–651. https://doi.org/10.1016/j.jcis.2020.09.059.

[9] J.F.L. Duval, Dynamics of metal uptake by charged biointerphases: bioavailability and bulk depletion, Phys. Chem. Chem. Phys. 15 (2013) 7873. https://doi.org/10.1039/c3cp00002h.

[10] J.F.L. Duval, H.P. van Leeuwen, R.M. Town, Electrostatic effects on ligand-assisted transfer of metals to (bio)accumulating interfaces and metal complexes (bioavai)lability, Colloids Surf. A Physicochem. Eng. Asp. 658 (2023) 130679. https://doi.org/10.1016/j.colsurfa.2022.130679.

[11] C. Pagnout, S. Jomini, M. Dadhwal, C. Caillet, F. Thomas, P. Bauda, Role of electrostatic interactions in the toxicity of titanium dioxide nanoparticles toward Escherichia coli, Colloids Surf. B. 92 (2012) 315–321. https://doi.org/10.1016/j.colsurfb.2011.12.012.

[12] C. Pagnout, A. Razafitianamaharavo, B. Sohm, C. Caillet, A. Beaussart, E. Delatour, I. Bihannic, M. Offroy, J.F.L. Duval, Osmotic stress and vesiculation as key mechanisms controlling bacterial

sensitivity and resistance to TiO2 nanoparticles, Commun. Biol. 4 (2021) 678. https://doi.org/10.1038/s42003-021-02213-y.

[13] T. Ikeda, C. Leidner, R.W. Murray, Kinetics of electron-transfer reactions of metal-complexes at impermeable redox active polymeric films on electrode surfaces and charge transport within the polymer film, J. Electroanal. Chem. 138 (1982) 343–365. https://doi.org/10.1016/0022-0728(82)85087-0.

[14] J.F.L. Duval, E. Sorrenti, Y. Waldvogel, T. Görner, P. de Donato, On the use of electrokinetic phenomena of the second kind for probing electrode kinetic properties of modified electron-conducting surfaces, Phys. Chem. Chem. Phys. 9 (2007) 1713–1729. https://doi.org/10.1039/b617422a.

[15] B. Lukanov, A. Firoozabadi, Specific ion effects on the self-assembly of ionic surfactants: A molecular thermodynamic theory of micellization with dispersion forces, Langmuir. 30 (2014) 6373–6383. https://doi.org/10.1021/la501008x.

[16] M.S. Santos, E.C. Biscaia, F.W. Tavares, Effect of electrostatic correlations on micelle formation, Colloids Surf. A Physicochem. Eng. Asp. 533 (2017) 169–178. https://doi.org/10.1016/j.colsurfa.2017.07.079.

[17] H. Wang, Q. Qin, X. Liang, Solving the nonlinear Poisson-type problems with F-Trefftz hybrid finite element model, Eng Anal Bound Elem. 36 (2012) 39–46. https://doi.org/10.1016/j.enganabound.2011.04.008.

[18] P. Batys, S. Luukkonen, M. Sammalkorpi, Ability of the Poisson-Boltzmann equation to capture molecular dynamics predicted ion distribution around polyelectrolytes, Phys. Chem. Chem. Phys. 19 (2017) 24583–24593. https://doi.org/10.1039/c7cp02547e.

[19] R. Tuinier, Approximate solutions to the Poisson-Boltzmann equation in spherical and cylindrical geometry, J. Colloid Interface Sci. 258 (2003) 45–49. https://doi.org/10.1016/S0021-9797(02)00142-X.

[20] K. Murota, T. Saito, Pore size effects on surface charges and interfacial electrostatics of mesoporous silicas, Phys. Chem. Chem. Phys. 24 (2022) 18073–18082. https://doi.org/10.1039/d2cp02520e.

[21] G. Trefalt, I. Szilagyi, M. Borkovec, Poisson-Boltzmann description of interaction forces and aggregation rates involving charged colloidal particles in asymmetric electrolytes, J Colloid Interface Sci. 406 (2013) 111–120. https://doi.org/10.1016/j.jcis.2013.05.071.

[22] E.J.W. Verwey, The electrical double layer and the stability of lyophobic colloids, Chem. Rev. 16 (1935) 363–415. https://doi.org/10.1021/cr60055a002.

[23] W. Bu, D. Vaknin, A. Travesset, How accurate is Poisson-Boltzmann theory for monovalent ions near highly charged interfaces ?, Langmuir. 22 (2006) 5673–5681. https://doi.org/10.1021/la053400e.

[24] T.Y. Lin, C.L. Chen, Analysis of electroosmotic flow with periodic electric and pressure fields via the lattice Poisson-Boltzmann method, Appl Math Model. 37 (2013) 2816–2829. https://doi.org/10.1016/j.apm.2012.06.032.

[25] I. Ermolina, H. Morgan, The electrokinetic properties of latex particles: Comparison of electrophoresis and dielectrophoresis, J Colloid Interface Sci. 285 (2005) 419–428. https://doi.org/10.1016/j.jcis.2004.11.003.

[26] D. Barten, J.M. Kleijn, J.F.L. Duval, H.P.V. Leeuwen, J. Lyklema, M.A.C. Stuart, Double layer of a gold electrode probed by AFM force measurements, Langmuir. 19 (2003) 1133–1139. https://doi.org/10.1021/la0117092.

[27] A.A. Kornyshev, Double-layer in ionic liquids: paradigm change ?, J. Phys. Chem. B. 111 (2007) 5545–5557. https://doi.org/10.1021/jp067857o.

[28] L. Belloni, Ionic condensation and charge renormalization in colloidal suspensions, Colloids Surf. A Physicochem. Eng. Asp. 140 (1998) 227–243.

[29] M. Bazant Z., B. Storey D., A. Kornyshev A., Double layer in ionic liquids: overscreening versus crowding, Phys. Rev. Lett. 106 (2011) 046102. https://doi.org/10.1103/PhysRevLett.106.046102.

[30] Y. Levin, Electrostatic correlations : from plasma to biology, Rep. Prog. Phys. 65 (2002) 1577. https://doi.org/10.1088/0034-4885/65/11/201.

[31] A. Kubíčková, T. Křiek, P. Coufal, M. Vazdar, E. Wernersson, J. Heyda, P. Jungwirth, Overcharging in biological systems: Reversal of electrophoretic mobility of aqueous polyaspartate by multivalent cations, Phys. Rev. Lett. 108 (2012) 186101. https://doi.org/10.1103/PhysRevLett.108.186101.

[32] P. Attard, Ion condensation in the electric double layer and the corresponding Poisson-Boltzmann effective surface charge, J. Phys. Chem. Lett. 99 (1995) 14174–14181.

[33] M. Quesada-Pérez, E. Gonzalez-Tovar, A. Martìn-Molina, M. Lozada-Cassou, R. Hidalgo-Alvarez, Overcharging in colloids: Beyond the Poisson-Boltzmann approach, Chemphyschem. 4 (2003) 234–248. https://doi.org/10.1002/cphc.200390040.

[34] P. Linse, V. Lobaskin, Electrostatic attraction and phase separation in solutions of like-charged colloidal particles, Phys. Rev. Lett. 83 (1999) 4208–4211. https://doi.org/10.1103/PhysRevLett.83.4208.

[35] K. Besteman, M.A.G. Zevenbergen, H.A. Heering, S.G. Lemay, Direct observation of charge inversion by multivalent ions as a universal electrostatic phenomenon, Phys. Rev. Lett. 93 (2004) 17. https://doi.org/10.1103/PhysRevLett.93.170802.

[36] D.J. Bonthuis, S. Gekle, R.R. Netz, Profile of the static permittivity tensor of water at interfaces: Consequences for capacitance, hydration interaction and ion adsorption, Langmuir. 28 (2012) 7679–7694. https://doi.org/10.1021/la2051564.

[37] J. Lyklema, Fundamentals of interface and colloid science. Volume II: Solid-liquid interfaces, Academic Press, London, 1995.

[38] H. Ohshima, T. Kondo, Relationship among the surface potential, Donnan potential and charge density of ion-penetrable membranes, Biophys. Chem. 38 (1990) 117–122. https://doi.org/10.1016/0301-4622(90)80046-A.

[39] A. Beaussart, C. Beloin, J.M. Ghigo, M.P. Chapot-Chartier, S. Kulakauskas, J.F.L. Duval, Probing the influence of cell surface polysaccharides on nanodendrimer binding to Gram-negative and Gram-positive bacteria using single-nanoparticle force spectroscopy, Nanoscale. 10 (2018) 12743–12753. https://doi.org/10.1039/c8nr01766b.

[40] C. Dika, M.H. Ly-Chatain, G. Francius, J.F.L. Duval, C. Gantzer, Non-DLVO adhesion of F-specific RNA bacteriophages to abiotic surfaces: Importance of surface roughness, hydrophobic and electrostatic interactions, Colloids Surf. A Physicochem. Eng. Asp. 435 (2013) 178–187. https://doi.org/I 10.1016/j.colsurfa.2013.02.045.

[41] S. Maurya, P. Gopmandal, H. Ohshima, J.F.L. Duval, Electrophoresis of composite soft particles with differentiated core and shell permeabilities to ions and fluid flow, J. Colloid Interface Sci. 558 (2020) 280–290. https://doi.org/10.1016/j.jcis.2019.09.118ï.

[42] R.J. Hill, D.A. Saville, “Exact” solutions of the full electrokinetic model for soft spherical colloids: Electrophoretic mobility, Colloids Surf. A Physicochem. Eng. Asp. 267 (2005) 31–49. https://doi.org/10.1016/j.colsurfa.2005.06.035.

[43] A. Beaussart, C. Caillet, I. Bihannic, R. Zimmermann, J.F.L. Duval, Remarkable reversal of electrostatic interaction forces on zwitterionic soft nanointerfaces in a monovalent aqueous electrolyte: an AFM study at the single nanoparticle level, Nanoscale. 10 (2018) 3181–3190. https://doi.org/10.1039/c7nr07976a.

[44] R. Zimmermann, J.F.L. Duval, C. Werner, J.D. Sterling, Quantitative insights into electrostatics and structure of polymer brushes from microslit electrokinetic experiments and advanced modelling of interfacial electrohydrodynamics, Curr Opin Colloid Interface Sci. 59 (2022) 101590. https://doi.org/10.1016/j.cocis.2022.101590.

[45] M. Moussa, C. Caillet, R.M. Town, J.F.L. Duval, Remarkable electrokinetic features of charge-stratified soft nanoparticles: Mobility reversal in monovalent aqueous electrolyte, Langmuir. 31 (2015) 5656–5666. https://doi.org/10.1021/acs.langmuir.5b01241.

[46] S. Chanda, S. Das, Effect of finite ion sizes in an electrostatic potential distribution for a charged soft surface in contact with an electrolyte solution, Phys. Rev. 89 (2014) 012307. https://doi.org/10.1103/PhysRevE.89.012307.

[47] P.P. Gopmandal, J.F.L. Duval, Electrostatics and electrophoresis of engineered nanoparticles and particulate environmental contaminants: Beyond zeta potential-based formulation, Curr Opin Colloid Interface Sci. 60 (2022) 101605. https://doi.org/10.1016/j.cocis.2022.101605.

[48] H. Ohshima, S. Ohki, Donnan potential and surface potential of a charged membrane, Biophys. J. 47 (1985) 673–678. https://doi.org/10.1016/S0006-3495(85)83963-1.

[49] C.N. Rochette, J.J. Crassous, M. Drechsler, F. Gaboriaud, M. Eloy, B. de Gaudemaris, J.F.L. Duval, Shell structure of natural rubber particles: Evidence of chemical stratification by electrokinetics and cryo-TEM, Langmuir. 29 (2013) 14655–14665. https://doi.org/10.1021/la4036858.

[50] A. Gupta, H.A. Stone, Electrical double layers: effects of asymmetry in electrolyte valence on steric effects, dielectric decrement, and ion-ionCorrelations, Langmuir. 34 (2018) 11971–11985. https://doi.org/10.1021/acs.langmuir.8b02064.

[51] P.H. Baudelet, G. Ricochon, M. Linder, L. Muniglia, A new insight into cell walls of Chlorophyta, Algal Res. 25 (2017) 333–371. https://doi.org/10.1016/j.algal.2017.04.008.

[52] J.F.L. Duval, H. Ohshima, Electrophoresis of diffuse soft particles, Langmuir. 22 (2006) 3533–3546. https://doi.org/10.1021/la0528293.

[53] J.F.L. Duval, R. Zimmermann, A.L. Cordeiro, N. Rein, C. Werner, Electrokinetics of diffuse soft interfaces. IV. Analysis of streaming current measurements at thermoresponsive thin films, Langmuir. 25 (2009) 10691–10703. https://doi.org/10.1021/la9011907.

[54] L.P. Yezek, J.F.L. Duval, H.P. van Leeuwen, Electrokinetics of diffuse soft interfaces. III. Interpretation of data on the polyacrylamide/water interface, Langmuir. 21 (2005) 6220–6227. https://doi.org/10.1021/la0580006.

[55] J.F.L. Duval, D. Küttner, M. Nitschke, C. Werner, R. Zimmermann, Interrelations between charging, structure and electrokinetics of nanometric polyelectrolyte films, J. Colloid Interface Sci. 362 (2011) 439–449. https://doi.org/10.1016/j.jcis.2011.06.063.

[56] C. Pagnout, R.M. Présent, P. Billard, E. Rotureau, J.F.L. Duval, What do luminescent bacterial metal-sensors probe? Insights from confrontation between experiments and flux-based theory, Sens. Actuators B Chem. 270 (2018) 482–491. https://doi.org/10.1016/j.snb.2018.05.033.

[57] S. Liu, K. Ghosh, M. Muthukumar, Polyelectrolyte solutions with added salt: A simulation study, J. Chem. Phys. 119 (2003) 1813–1823. https://doi.org/10.1063/1.1580109.

940 [58] R. Zimmermann, D. Romeis, I. Bihannic, M. Cohen Stuart, J.U. Sommer, C. Werner,
941 Electrokinetics as an alternative to neutron reflectivity for evaluation of segment density
942 distribution in PEO brushes, Soft Matter. 10 (2014) 7804–7809.
943 https://doi.org/10.1039/c4sm01315h.
944 [59] S.M. Kilbey, J.F. Ankner, Neutron reflectivity as a tool to understand polyelectrolyte brushes,
945 Curr Opin Colloid Interface Sci. 17 (2012) 83–89. https://doi.org/10.1016/j.cocis.2011.08.007.
946 [60] R. Zimmermann, D. Kuckling, M. Kaufmann, C. Werner, J.F.L. Duval, Electrokinetics of a poly(N-
947 isopropylacrylamid- co-carboxyacrylamid) soft thin film: Evidence of diffuse segment
948 distribution in the swollen state, Langmuir. 26 (2010) 18169–18181.
949 https://doi.org/10.1021/la103526b.
950 [61] J.J. Bikerman, XXXIX. Structure and capacity of electrical double layer, The London, Edinburgh,
951 and Dublin Philosophical Magazine and Journal of Science. 33 (1942) 384–397.
952 [62] M.S. Kilic, M.Z. Bazant, Steric effects in the dynamics of electrolytes at large applied voltages . I
953 . Double-layer charging, Phys. Rev. 75 (2007) 021502.
954 https://doi.org/10.1103/PhysRevE.75.021502.
955 [63] R.M. Adar, T. Markovich, A. Levy, H. Orland, D. Andelman, Dielectric constant of ionic solutions:
956 Combined effects of correlations and excluded volume, J. Phys. Chem. 149 (2018) 054504.
957 https://doi.org/10.1063/1.5042235.
958 [64] J.B. Hasted, D.M. Ritson, C.H. Collie, Dielectric properties of aqueous ionic solutions. Parts I and
959 II, J. Chem. Phys. 16 (1948) 1.
960 [65] D.C. Grahame, Effects of dielectric saturation upon the diffuse double layer and the free energy
961 of hydration of ions, J. Chem. Phys. 18 (1950) 903–909. https://doi.org/10.1063/1.1747807.
962 [66] J.J. López-García, M.J. Aranda-Rascón, J. Horno, Electrical double layer around a spherical
963 colloid particle: The excluded volume effect, J. Colloid Interface Sci. 316 (2007) 196–201.
964 https://doi.org/10.1016/j.jcis.2007.07.054.
965 [67] Y. Nakayama, D. Andelman, Differential capacitance of the electric double layer: The interplay
966 between ion finite size and dielectric decrement, J. Chem. Phys. 142 (2015) 044706.
967 https://doi.org/10.1063/1.4906319.
968 [68] R. Kjellander, D.J. Mitchell, Dressed-ion theory for electrolyte solutions: A Debye-Hückel-like
969 reformulation of the exact theory for the primitive model, J. Chem. Phys. 101 (1994) 603–626.
970 https://doi.org/10.1063/1.468116.
971 [69] R.M. Adar, S.A. Safran, H. Diamant, D. Andelman, Screening length for finite-size ions in
972 concentrated electrolytes, Phys. Rev. E. 100 (2019) 042615.
973 https://doi.org/10.1103/PhysRevE.100.042615.

[70] J.W. Cahn, J.E. Hilliard, Free energy of a nonuniform system . I. Interfacial free energy, J. Chem. Phys. 28 (1958) 258.

[71] S.S. Barman, S. Bhattacharyya, Finite ion size and ion permittivity effects on gel electrophoresis of a soft particle, Colloids Surf. A Physicochem. Eng. Asp. 636 (2022) 128088. https://doi.org/10.1016/j.colsurfa.2021.128088.

[72] U. Ascher, J. Christiansen, R.D. Russell, Collocation Software for Boundary-Value ODEs, ACM Trans. Math. Softh. 7 (1981) 223–22.

[73] M. Mezger, H. Schröder, H. Reichert, S. Schramm, J.S. Okasinski, S. Schöder, V. Honkimäki, M. Deutsch, B.M. Ocko, J. Ralston, M. Rohwerder, M. Stratmann, H. Dosch, Molecular layering of fluorinated lonic liquids at a charged sapphire (0001) surface, Science (1979). 322 (2008) 424–428. https://doi.org/10.1126/science.1164502.

[74] B.D. Storey, M.Z. Bazant, Effects of electrostatic correlations on electrokinetic phenomena, Phys. Rev. 86 (2012) 056303. https://doi.org/10.1103/PhysRevE.86.056303.

[75] J.F.L. Duval, C. Werner, R. Zimmermann, Electrokinetics of soft polymeric interphases with layered distribution of anionic and cationic charges, Curr Opin Colloid Interface Sci. 24 (2016) 1–12. https://doi.org/10.1016/j.cocis.2016.05.002.

[76] P.A. Gomes, J.-B. d'Espinose de Lacaillerie, B. Lartiges, M. Maliet, V. Molinier, N. Passade-Boupat, N. Sanson, Microalgae as Soft Permeable Particles, Langmuir. 38 (2022) 14044–14052. https://doi.org/10.1021/acs.langmuir.2c01735.

[77] K. Li, W. Wang, F. Xiao, Y. Ge, H. Jin, Z. Yu, J. Gong, W. Gao, Z. Peng, Atomic force microscopy study of non-DLVO interactions between drops and bubbles, Langmuir. 37 (2021) 6830–6837. https://doi.org/10.1021/acs.langmuir.1c00937.

[78] J.F.L. Duval, S. Bera, L.J. Michot, J. Daillant, L. Belloni, O. Konovalov, D. Pontoni, X-ray reflectivity at polarized liquid-Hg-aqueous-electrolyte interface: Challenging macroscopic approaches for ion-specificity issues, Phys. Rev. Lett. 108 (2012) 206102. https://doi.org/10.1103/PhysRevLett.108.206102.

[79] R. Paul, D. Maity, P. Agrawal, A. Bandopadhyay, S. Chakraborty, Electrokinetics of non-Newtonian fluids in poly-electrolyte grafted nanochannels: Effects of ion-partitioning and confinement, J Nonnewton Fluid Mech. 283 (2020) 104348. https://doi.org/10.1016/j.jnnfm.2020.104348.

[80] K. Singh, A. Raghav, P.K. Jha, S. Satapathi, Effect of size and charge asymmetry on aggregation kinetics of oppositely charged nanoparticles, Sci. Rep. 9 (2019) 3762. https://doi.org/10.1038/s41598-019-40379-y.